

Fluctuation Theorems for Heat exchanges between passive and active baths

Massimiliano Semeraro^{1*}, Antonio Suma¹ and Giuseppe Negro¹

¹Dipartimento di Fisica, Università degli Studi di Bari and INFN, Sezione di Bari, via Amendola 173, 70126 Bari, Italy

E-mail: * massimiliano.semeraro@uniba.it

Abstract. In addition to providing general constraints on probability distributions, fluctuation theorems allow to infer essential information on the role played by temperature in heat exchange phenomena. In this numerical study, we measure the temperature of an out of equilibrium active bath using a fluctuation theorem that relates the fluctuations of the heat exchanged between two baths to their temperatures. Our setup consists of a single particle moving between two wells of a quartic potential accommodating two different baths. The heat exchanged between the two baths is monitored according to two definitions: as the kinetic energy carried by the particle whenever it jumps from one well to the other and as the work performed by the particle on one of the two baths when immersed in it. First, we consider two equilibrium baths at two different temperatures and verify that a fluctuation theorem featuring the baths temperatures holds for both heat definitions. Then, we introduce an additional Gaussian coloured noise in one of the baths, so as to make it effectively an active (out-of-equilibrium) bath. We find that a fluctuation theorem is still satisfied with both heat definitions. Interestingly, in this case the temperature obtained through the fluctuation theorem for the active bath corresponds to the kinetic temperature when considering the first heat definition, while it is larger with the second one. We interpret these results by looking at the particle jump phenomenology.

Keywords: heat exchange, out-of-equilibrium systems, fluctuation theorem, active bath, out-of-equilibrium temperatures

1. Introduction

A fundamental open issue in statistical physics is the extension of the equilibrium framework to out of equilibrium settings. Amongst the many questions still waiting for an answer, the definition of a proper temperature that consistently regulates *heat fluctuations and exchanges* between out of equilibrium thermal baths posits a central problem. For glassy systems, whose non-equilibrium character is due to very long relaxational times [1, 2], an effective thermal picture has already emerged. Here an effective temperature can in fact be defined using the non-equilibrium deviations of the fluctuation-dissipation theorem [3, 4]. One then naturally wonders if a similar scenario applies also to other classes out of equilibrium systems.

One class of out of equilibrium systems that in the past few years attracted great interest is *active matter* [5–17]. The distinctive feature of all systems from this class is a continuous conversion and injection of energy from internal reservoirs or the surrounding environment into the system itself to produce self propulsion of its minimal constituents. Interestingly, the mere introduction of a self-propulsion mechanism results in a wealth of new phenomena and features, as for example collective motion [13, 18–21], motility-induced phase separation [22–24] a rich phase diagram [25–28] and dynamical phase transitions [29–31], most of which have no equivalent in passive counterparts. According to stochastic thermodynamics [32–34], the injection of energy is an irreversible process which makes active systems inherently out of equilibrium [35, 36]. As a consequence, the Stokes-Einstein relation between injection and dissipation of energy is naturally violated at microscopic scales [37–39], therefore making active matter systems a perfect stage for introducing and testing different definitions of out of equilibrium temperatures. In this respect, we mention that there have been several attempts to describe this inherent non-equilibrium character at macroscopic scales through the introduction of an effective temperature [40–48]. However, up to our knowledge, a general effective thermal picture has not yet emerged.

An approach that can be exploited to test at mesoscopic level different definitions of out of equilibrium temperatures is offered by the so called *fluctuation theorems*, i.e. universal constraints on the probability distribution of integrated observables like work, heat and entropy production evaluated along the trajectories of individual physical entities of the system of interest [32, 49–54]. An important result showing that temperatures naturally enter heat fluctuation theorems is provided by [55], in which it was shown that the heat exchanged between two equilibrium thermal baths satisfies the following fluctuation theorem

$$I(-q) - I(q) = \left(\frac{1}{T_1} - \frac{1}{T_2} \right) q, \quad (1)$$

where q is the heat exchanged per unit time, $I(q) \equiv \lim_{t \uparrow \infty} -\log P(q)/t$ is its associated Rate Function from Large Deviation Theory [56–58] and T_1, T_2 coincide with the bath temperatures. The above result was later studied in the context of Brownian particles [59, 60], finding that its validity is in general restricted to finite intervals of q . The fluctuation theorem Equation 1 represents a natural starting point for an investigation on the values T_1 and T_2 could take in (possibly still valid) fluctuation theorems in out of equilibrium contexts, where fluctuations are central. The temperatures defined from a fit of Equation 1 and denoted as T_{FT} can in fact be compared with other significant definitions of temperatures, such as the *effective temperature*, denoted as T_{eff} and defined from the deviation of the fluctuation-dissipation theorem [3, 4, 46, 61–65], or the *kinetic temperature*, instead denoted as T_{kin} and defined from the equipartition theorem [4, 48, 64, 66] (see Appendix Appendix A for more details).

Here, we numerically investigate the definition of T_{FT} by considering an idealized setup which consists in a single one-dimensional particle moving in a quartic double well

potential (see Figure 1 for a schematic depiction). In each well the particle is put in contact with a different overall thermal bath, thus experiencing a different temperature. In the right well we place an equilibrium thermal bath which is formalized through a Gaussian zero-mean delta-correlated white noise plus a viscous friction force and satisfies a usual fluctuation-dissipation theorem with an effective temperature trivially coinciding with both the bath and the kinetic ones. For the left well bath we instead consider two different cases: first we fix a further equilibrium thermal bath with same characteristics as the one in the right well expect for a different temperature; then we make it an active bath by fixing an equilibrium thermal bath analogous to the one from the right well, now with same temperature, and introducing an Ornstein-Uhlenbeck process playing the role of an additional Gaussian coloured noise with exponential self-correlation. In this way, when in the left well, the particle effectively turns into an active particle, more specifically an Active Ornstein-Uhlenbeck particle [67–70]. Moreover we remark that in this case neither the usual fluctuation-dissipation theorem is satisfied [38] nor kinetic and effective temperatures coincide [48]. The heat exchanged is measured according to two different definitions: as the work performed by one of the two baths on the particle and as the sum of the kinetic energies carried by the particle every time it jumps from one well to the other. The first definition is nothing but the usual heat as defined in the framework of stochastic thermodynamics [33, 71]. The second one is instead newly introduced as suggested by our specific setup.

We find that in all cases considered the fluctuation theorem Equation 1 is still valid. More in detail, in the case in which two equilibrium thermal baths with different temperatures are fixed, both definitions of heat exchanged lead to the validity of Equation 1 with slope in accordance with the bath temperatures. This first result provides an essential correspondence between T_{FT} and both T_{eff} and T_{kin} which, as mentioned above, in this case both trivially coincide with the bath ones. In the active bath case, we find instead that different values of T_{FT} associated to the active bath emerge based on the definition of heat under study. When the heat as sum of kinetic energies is considered, the extracted T_{FT} turns out to correspond to the kinetic temperature of the active bath. When instead considering the heat as the work performed by the thermal environment, this temperature assumes intermediate values between the kinetic temperature and the effective one. These results and discrepancies can be interpreted by looking at the particle jump phenomenology.

The remainder of the paper is structured as follows. In section 2 we present the model and methods we adopted. In particular, in subsection 2.1 we describe our setup and detail the two cases under scrutiny, in subsection 2.2 we introduce the two definitions of heat exchanged we consider along with the energy balance of the system, in subsection 2.3 we describe the numerical methods we adopted and in subsection 2.4 we comment on the stationary position distribution of the system. Next, in section 3 we present and comment the results of our investigation for the two bath configurations considered. Finally, in section 4 we report our closing remarks.

2. Model and Methods

2.1. Model

The general framework of our setup is that of a unidimensional unit-mass mesoscopic particle of position $x(t)$ and diameter $\sigma = 1$ moving under the action of the external quartic double well potential

$$U(x(t)) = \frac{a}{4} (x(t) - x_u)^4 - \frac{b}{2} (x(t) - x_u)^2, \quad (2)$$

where $a, b > 0$ and x_u is the centre of the potential which we set to zero and serves as separating point between the regions $x > x_u$ (*right well*) and $x \leq x_u$ (*left well*) where thermal baths with different features act. The local maximum of the potential is located at $x_u = 0$, the global minima are at $\pm x_m = x_u \pm \sqrt{b/a}$ distanced by $2\sqrt{b/a}$ and its depth $\Delta U = U(x_u) - U(\pm x_m) = b^2/4a$ represents the height of the barrier the particle has to overcome to hop from one well to the other. In order to highlight the spatial separation of the two baths induced by the potential Equation 2, we recast the usual Langevin equation describing the particle dynamics with initial conditions $x(0) \equiv x_0$ and $\dot{x}(0) \equiv v_0$ into the following form

$$\ddot{x}(t) = B_1(\dot{x}(t), t)\theta(x(t)) + B_2(\dot{x}(t), t)(1 - \theta(x(t))) - \frac{dU[x(t)]}{dx}, \quad (3)$$

where $B_1(\dot{x}(t), t)$ and $B_2(\dot{x}(t), t)$ collect the forces exerted by the overall baths in the two wells. The presence of the Heaviside functions $\theta(x(t))$ ensures in fact $B_1(\dot{x}(t), t)$ and $B_2(\dot{x}(t), t)$ to act only when the particle is in the right or left well, respectively[‡]. Concerning instead the action of the baths, whenever the particle hops into each of the two wells, their corresponding noise processes are made to restart acting with an initial condition extracted from their stationary distributions. Figure 1 graphically summarizes our setup highlighting with different colours the left and right well regions.

We now specify the actual composition of the forces contributing to each bath. In the right well, $B_1(\dot{x}(t), t)$ is always associated to a usual equilibrium thermal bath, hereafter referred to as *passive bath*, thus

$$B_1(\dot{x}(t), t) = -\gamma\dot{x}(t) + \sqrt{2\gamma T_1} \xi_1(t), \quad (4)$$

where γ is the viscous friction coefficient, T_1 is the bath temperature and $\xi_1(t)$ is a usual Gaussian white noise with $\langle \xi_1(t) \rangle = 0$ and $\langle \xi_1(t)\xi_1(t') \rangle = \delta(t - t')$. Note that, for the sake of simplicity, here and in the following we set the Boltzmann constant k_B to unity. The distribution for the restart of $\xi_1(t)$ is then a normal Gaussian $\mathcal{N}(0, 1)$. As aforementioned, for the bath in the left well we instead distinguish two different cases:

[‡] For the sake of simplicity, here we assume the convention $\theta(0) = 0$ [72] instead of the half-maximum one $\theta(0) = 1/2$ [73] so that the function is left-continuous at $x = 0$ and $\theta(t)$ and $1 - \theta(t)$ can be properly considered as the indicator functions of the intervals $(0, +\infty)$ and $(-\infty, 0]$, respectively. We underline that this choice does not affect our results as the value of a function at a single point does not affect the overall values of the heat integrals from subsection 2.2.

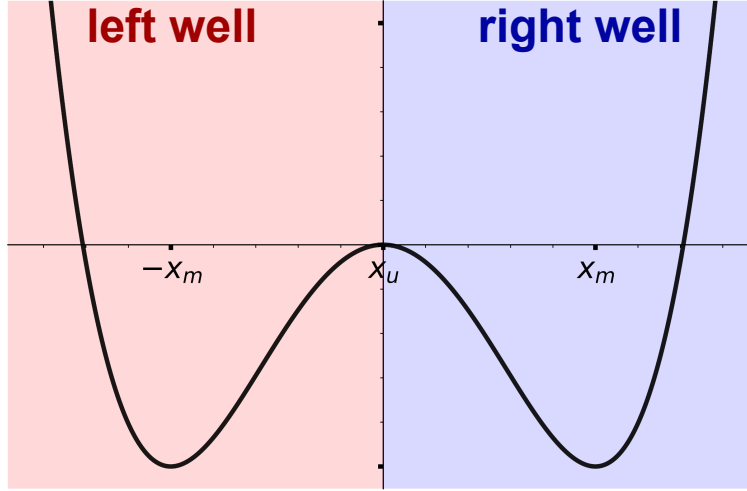


Figure 1. Schematic depiction of our idealized setup. The black line denotes the quartic double well potential Equation 2 with minima and local maxima at $\pm x_m$ and x_u , respectively, and depth ΔU , the red and blue areas and labels below and above x_u denote the action of baths with different features in the two wells and the gray circle denotes the Brownian particle while jumping from the left to the right well, as suggested by the black arrow.

- a) another passive bath with friction coefficient γ and temperature T_2 , i.e.

$$B_2(\dot{x}(t), t) = -\gamma\dot{x}(t) + \sqrt{2\gamma T_2} \xi_2(t) , \quad (5)$$

where $\xi_2(t)$ is a Gaussian white noise independent on $\xi_1(t)$ with $\langle \xi_2(t) \rangle = 0$, $\langle \xi_2(t)\xi_2(t') \rangle = \delta(t - t')$ and T_2 in general different from T_1 . As for $\xi_1(t)$, the distribution for the restart of $\xi_2(t)$ is $\mathcal{N}(0, 1)$. Note that in this specific case the temperature for the entire domain can be written as the x -dependent function $T(x) \equiv T_2 + (T_1 - T_2)\theta(x)$, so that the overall Langevin equation Equation 3 can be recast as

$$\ddot{x}(t) = -\gamma\dot{x}(t) + \sqrt{2\gamma T[x(t)]} \xi(t) - \frac{dU[x(t)]}{dx(t)} , \quad (6)$$

where $\xi(t)$ is a single Gaussian white noise with $\langle \xi(t) \rangle = 0$ and $\langle \xi(t)\xi(t') \rangle = \delta(t - t')$ acting everywhere in the system which is made multiplicative by the presence of $T(x)$ in its multiplicative factor;

- b) a passive bath with friction coefficient γ and temperature T_2 and an additional *Ornstein-Uhlenbeck noise* reminiscent of the active force from the active Ornstein-Uhlenbeck particle model [67–70] and hereafter referred to as *active bath*, i.e.

$$B_2(\dot{x}, t) = -\gamma\dot{x}(t) + \sqrt{2\gamma T_2} \xi_2(t) + a(t) , \quad (7)$$

where $\xi_2(t)$ is a Gaussian white noise analogous to the one from case a) and $a(t)$ is an Ornstein-Uhlenbeck process implemented as the solution of the additional

stochastic differential equation

$$\dot{a}(t) = -\gamma_R a(t) + F_a \sqrt{2\gamma_R} \eta(t) \quad (8)$$

with initial condition $a(0) \equiv a_0$, where $\eta(t)$ is a further Gaussian white noise independent on both $\xi_1(t)$ and $\xi_2(t)$ with $\langle \eta(t) \rangle = 0$ and $\langle \eta(t)\eta(t') \rangle = \delta(t-t')$ and γ_R^{-1} and F_a are the *persistence time* associated to the the active process and a positive constant ruling its magnitude, respectively. From the average and self-correlation of $a(t)$

$$\langle a(t) \rangle = a_0 e^{-\gamma_R t} \quad \text{and} \quad \langle a(t)a(t') \rangle = a_0^2 e^{-\gamma_R(t+t')} + F_a^2 \left(e^{-\gamma_R|t-t'|} - e^{-\gamma_R(t+t')} \right), \quad (9)$$

one in fact immediately realizes that $\tau_p = \gamma_R^{-1}$ controls the exponential decay of both average and self-correlations and that at large times $\langle a^2(t) \rangle \simeq F_a^2$, so that F_a indeed plays the role of average magnitude for the active process [68, 70, 74]. Equation 9 also suggests that the distributions for the restart of $\xi_2(t)$ and $a(t)$ are $\mathcal{N}(0, 1)$ and $\mathcal{N}(0, F_a^2)$, respectively. In order to better discern the action of $a(t)$, here we fix $T_1 = T_2$ and, for the sake of simplicity we also set $\gamma_R = 3T_2/(\gamma\sigma^2)$ [24, 31, 75]. Moreover, as typically done [23–25, 31, 66, 75], we control the relative magnitude activity-thermal noise varying the adimensional Péclet number

$$Pe \equiv \frac{F_a \sigma}{T_2}, \quad (10)$$

where we recall $\sigma = 1$ to be the particle diameter. We remark that in general, the active bath configuration can be realized in actual experiments making use of Janus particles [76–79] or and optical tweezers [80, 81], or also introducing a passive tracer particle in a suspension of active particles whose collisions with the tracer itself can be described by $a(t)$ [54, 82].

Finally, in order to allow the particle to correctly thermalize in each well before every jump, we need to correctly assess the relevant timescales of the system. Concerning case a), there are only two relevant timescales. The first one is the *inertial time* $\tau_I = \gamma^{-1}$, which is the typical time needed to attain thermal equilibrium with the bath. The second one is the average time the particle remains in one well before hopping starting the barrier ascension from $\pm x_m$, or *average residence time*, τ_r . In the overdamped limit for a single white-noise bath acting everywhere and a parameter choice such that $\Delta U/T \gg 1$, τ_r is estimated as [83]

$$\tau_r = \frac{\pi\gamma}{\sqrt{U''(x_m)|U''(x_0)|}} e^{\frac{\Delta U}{T}} = \frac{\pi\gamma}{\sqrt{2b}} e^{\frac{\Delta U}{T}}, \quad (11)$$

where $U''(x(t))$ is the second derivative of the potential Equation 2. In order to allow the particle to thermalize after each jump we require $\tau_r > \tau_I$ in each well. In the following we use the symbols τ_r^l and τ_r^r to denote the average residence times in the left and right well, respectively. Concerning case b) yet another timescale needs

to be considered: the persistence time $\tau_p = \gamma_R^{-1}$ controlling the exponential decay of the coloured noise correlations. A further condition that is required to let the particle thermalise in presence of the additional Ornstein-Uhlenbeck force is then $\tau_r > \tau_p$. We remark that in presence of an active process like $a(t)$ a Kramers-like formula similar to Equation 11 for τ_p is still in place in some limiting conditions [84]. However, we checked in our settings that such a formula does not hold, thus forcing us to resort to numerical estimations.

2.2. Definitions of Heat Exchanged and Energy Balance

Our primary interest focuses on the heat exchanged between the two wells as the particle hops between them, which here we sample according to two different definitions capturing each different physical aspects of the system.

The first definition we consider relies on the intuitive idea that exchanges of energy and heat between the two baths must be somehow be related to the jumps of the particle from one well to the other. More in detail, each of the $N_E \geq 0$ jumps occurring during a time interval of duration τ can be considered as an event of instantaneous transfer of kinetic energy from one bath to the other, with the particle playing the role of carrier. Therefore, an intuitive way in which we define the energy exchange between the two is as

$$\mathcal{Q}_E^R \equiv \frac{1}{2} \sum_{j=1}^{N_E} |\dot{x}(\tau_j)| \dot{x}(\tau_j) . \quad (12)$$

We would like to stress that the above formula is simply configured as the sum of the kinetic energies carried during each jump by the particle, i.e. a simple quantitative version of the intuitive idea delineated above. Here the subscript E denotes the energetic origin of this definition, while $\{\tau_j\}_{j=1, \dots, N_E}$ is the succession of times during the sampling interval of duration τ in which all jumps events occur, i.e. at which $x(t) = x_u$. Note that the absolute value in Equation 12 ensures the increments of \mathcal{Q}_E to be given a proper sign depending on the direction of each jump event. For the right well they are in fact positive (negative) when the particle jumps from left (right) to right (left), coherently with the physical intuition that the right well bath receives (loses) energy when the particles enters in (goes away from) it. In order to remain faithful to the prescription that a bath acquires (loses) energy when the particle jumps in (away from) it, when focusing on the left well we need to invert our point of view. In particular, now the increments of \mathcal{Q}_E^L must be considered negative (positive) when the particle jumps from left (right) to right (left). In terms of the total energy exchange \mathcal{Q}_E^L , this translates into an overall minus sign with respect to \mathcal{Q}_E^R , i.e. $\mathcal{Q}_E^L = -\mathcal{Q}_E^R$. Trivially, $\mathcal{Q}_E^L + \mathcal{Q}_E^R = 0$.

The second definition we consider takes up the usual one provided by stochastic thermodynamics in which heat is defined as the work performed on the particle by the passive bath, i.e. viscous friction force plus white noise [33, 71]. In our specific setting, the definition for the heat exchanged between particle and passive bath during a time

interval of duration τ in the right well transforms into

$$\begin{aligned}
 \mathcal{Q}_W^R &\equiv - \int_0^\tau B_1(\dot{x}(s), s) \theta(x(s)) \circ dx(s) \\
 &= - \sum_{j=1}^{N_R} \int_{\tau_{0,j}}^{\tau_{R,j}} B_1(\dot{x}(s), s) \dot{x}(s) ds \\
 &= - \sum_{j=1}^{N_R} \int_{\tau_{0,j}}^{\tau_{R,j}} (-\gamma \dot{x}(s) + \sqrt{2\gamma T_1} \xi_1(s)) \dot{x}(s) ds
 \end{aligned} \tag{13}$$

where the symbol \circ denotes the Stratonovich prescription is adopted [85], the sign minus denotes that it is the particle to perform work on the bath and ensures the same sign convention as for \mathcal{Q}_E^R to be fulfilled, the subscript W highlights the thermodynamical origin of this definition, N_R denotes the number of times the particle resides in the right well and $\tau_{0,j}, \tau_{R,j}$, $j = 1, \dots, N_R$ denote the beginning and ending times of the j -th residency in the well, respectively, with $\tau_{R,j} - \tau_{0,j} > 0$ its duration.

In order to provide physical intuition about the difference between the heat definitions from Equation 12 and Equation 13, in panel **(a)** of Figure 2 we show a typical particle trajectory in case a), while in panel **(b)** we show the corresponding realisations of \mathcal{Q}_E^R and \mathcal{Q}_W^R during the same time interval (numerical data are obtained using the numerical techniques described in subsection 2.3). Note that \mathcal{Q}_E^R is piecewise continuous and presents discontinuous variations only when jump events occur, while \mathcal{Q}_W^R continuously evolves when the particle is in the right well remaining constant when the particle jumps in the left well and showing significant variations only when jump events occur. Note also that during the first permanence of the particle in the left well \mathcal{Q}_W^R averages to zero, coherently with the fact that during this time interval the particle is thermalized with the right-well bath and the latter has not yet received any energy injection from the left-well bath.

Following standard procedures, from Equation 13 the trajectory-wise energy balance of the system can be obtained [33, 71]. By simply using the Langevin equation Equation 3 to replace $B_1(\dot{x}(t), t)\theta(x(t))$ in Equation 13 for generality in case b) and adopting the Stratonovich prescription to perform integrals [85], one in fact finds

$$\begin{aligned}
 \frac{1}{2} \Delta \dot{x}^2(\tau) + \Delta U(x(\tau)) &= \int_0^\tau B_1(\dot{x}(s), s) \theta(x(s)) \dot{x}(s) ds + \int_0^\tau B_2(\dot{x}(s), s) (1 - \theta(x(s))) \dot{x}(s) ds \\
 &= -\mathcal{Q}_W^R - \mathcal{Q}_W^L + \mathcal{W}_a,
 \end{aligned} \tag{14}$$

where $\int_0^\tau \ddot{x}(s) \dot{x}(s) ds = (\dot{x}^2(\tau) - \dot{x}^2(0))/2 \equiv \frac{1}{2} \Delta \dot{x}^2(\tau)$ and $\int_0^\tau \frac{dU(x(s))}{dx(s)} \dot{x}(s) ds = (U(x(\tau)) - U(x(0))) \equiv \Delta U(x(\tau))$ respectively denote the variation of kinetic and potential energy from initial configuration at $t = 0$ and final one at $t = \tau$, \mathcal{Q}_R^W denotes the work performed by the particle on the right passive bath defined in Equation 13,

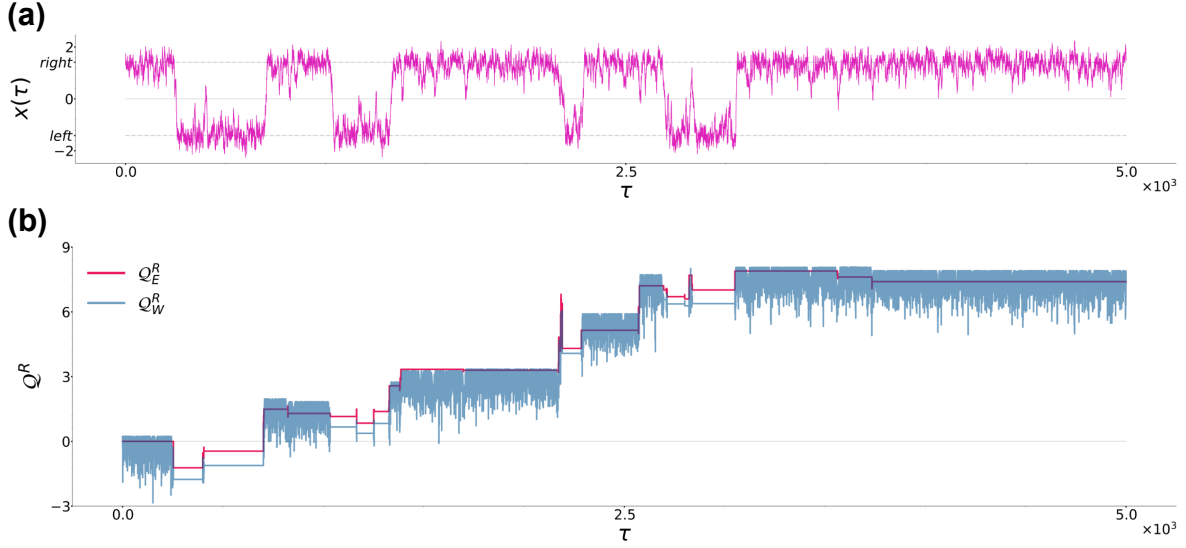


Figure 2. (a): typical trajectory of a Brownian particle from case a) at sampling time $\tau = 5 \cdot 10^3$. The black dashed lines denote the location of the left and right potential minima at $\pm x_m = \pm \sqrt{b/a} = \pm \sqrt{2}$. (b): time evolution of \mathcal{Q}_E^R and \mathcal{Q}_W^R corresponding to the trajectory in panel (a). Parameters are $a = 1.0$, $b = 2.0$, $\gamma = 10$, $T_1 = 0.2$ and $T_2 = 0.3$.

and

$$\begin{aligned} \mathcal{Q}_W^L &\equiv - \int_0^\tau (-\gamma \dot{x}(s) + \sqrt{2\gamma T_2} \xi_2(s))(1 - \theta(x(s))) \circ dx(s) \\ &= - \sum_{j=1}^{N_L} \int_{\tau_{0,j}}^{\tau_{L,j}} (-\gamma \dot{x}(s) + \sqrt{2\gamma T_2} \xi_2(s)) \dot{x}(s) ds \end{aligned} \quad (15)$$

denotes the work performed by the particle on the passive component of the left bath only, i.e. friction force plus white noise, with N_L the number of times the particle resides in the left well and $\tau_{0,j} < \tau_{L,j}$ beginning and ending times of each of the j -th residencies, and finally

$$\mathcal{W}_a \equiv \int_0^\tau a(s)(1 - \theta(x(s))) \circ dx(s) = \sum_{j=1}^{N_L} \int_{\tau_{0,j}}^{\tau_{L,j}} a(s) \dot{x}(s) ds \quad (16)$$

denotes the active work, i.e. the work performed by the additional noise in the left well returning the energy cost to sustain the particle self propulsion [31, 54, 70, 86, 87]. In both Equation 15 and Equation 16 \circ again underlies the Stratonovich prescription. We point out that $\mathcal{Q}_W^{R,L}$ and \mathcal{W}_a are energy contributions extensive in time, while the variation of both kinetic and potential energies $\Delta \dot{x}^2(\tau)/2$ and $\Delta U(x(\tau))$ are not, i.e.

$$\lim_{\tau \uparrow \infty} \frac{1}{\tau} \int_0^\tau d \left(\frac{1}{2} \dot{x}^2(t) + U(x(t)) \right) = 0, \quad (17)$$

or, by assuming ergodicity,

$$\frac{d}{dt} \left\langle \frac{1}{2} \dot{x}^2(t) + U(x(t)) \right\rangle = 0, \quad (18)$$

where the derivative is zero due to $\langle \dot{x}^2(t)/2 + U(x(t)) \rangle$ assuming a constant value independent of t . As a consequence, when passing to the energy balance per unit time, at times much larger than all relevant timescales of the system one has

$$0 = -q_W^R - q_W^L + w_a. \quad (19)$$

where $q = \mathcal{Q}/\tau$ for all sub- and superscripts and $w = \mathcal{W}_a/\tau$. Note that, coherently with the fact that the system under consideration is globally isolated, Equation 19 shows the overall energies exchanged by the two baths, $-q_W^R$ for the right and $-q_W^L + w_a$ for the left one, to be of opposite sign and sum to zero.

Finally, a few comments and remarks. We underline that case a) does not include the additional noise $a(t)$, so that $\mathcal{W}_a = 0$ and Equation 14 reduces to the usual equivalence between energy variation of the system and heat exchanged. We would also like to stress that in case b) \mathcal{Q}_W^L does not capture the heat exchanges related to the left bath in its entirety. As $-\int_0^\tau B_2(\dot{x}(s), s)\dot{x}(s)(1 - \theta(x(s))) ds = \mathcal{Q}_W^L - \mathcal{W}_a$, the latter in fact also includes the active work contribution. Nevertheless, as shown in subsection 3.2, \mathcal{Q}_W^L is indirectly influenced by the action of the active noise as the latter clearly affects the particle velocity in the left well. In this respect, we remark that, as the active noise $a(t)$ pushes the particle, it is very likely for $a(t)$ and $\dot{x}(t)$ to have the same sign so that \mathcal{W}_a from Equation 16 is very unlikely to be negative. Finally, referring to the trajectory of \mathcal{Q}_W^R relative to case a) from Figure 2(b), we conclude by pointing out that during each permanence of the particle in the right well \mathcal{Q}_W^R is bounded from above by a different value. In order to prove this point, let us consider a particle which has jumped into the right well the last time at τ_J and up to time $\tau > \tau_J$ remained in it. Then one has

$$\begin{aligned} \mathcal{Q}_W^R &= c_q - \int_{\tau_J}^\tau (-\gamma\dot{x}(s) + \sqrt{2\gamma T_1} \xi_1(s))\dot{x}(s) ds \\ &= \left(\frac{1}{2} \dot{x}^2(\tau_J) + U(x(\tau_J)) \right) - \left(\frac{1}{2} \dot{x}^2(\tau) + U(x(\tau)) \right) + c_q \\ &\leq \frac{1}{2} \dot{x}^2(\tau_J) + U(x(\tau_J)) - U_m + c_q, \end{aligned} \quad (20)$$

where in the first row we used the definition Equation 13 and c_q records the value accumulated by \mathcal{Q}_W^R up to time τ_J , in the second row we instead used the Langevin equation Equation 3 and performed integration similarly to the case of Equation 14 and finally in the third row we used the lower bounds $\dot{x}^2(\tau)/2 \geq 0$ and $U(x(\tau)) \geq U(\pm x_m) \equiv U_m$. Interestingly, the bound of \mathcal{Q}_W^R from Equation 20 comes to depend on c_q , which englobes the integration of \mathcal{Q}_W^R up to time τ_J , on the potential energy U_m at the minimum and also on the kinetic and potential energies evaluated exactly at τ_J , i.e. when the particle last entered into the right well.

2.3. Numerical Methods and Parameters

The numerical integration of Equation 3 and Equation 8 is performed via the velocity-Verlet [88] and the Euler-Maruyama [89] integrators, respectively, with integration timestep $dt = 10^{-2}$ in both cases. We choose for the quartic potential Equation 2 $a = 1$ and $b = 2$, setting then a distance between minima and a barrier height of $2\sqrt{2}$ and $\Delta U = 1$, respectively. Along with the unitary particle mass and diameter σ , the barrier height ΔU set the reduced units of our simulations. In all cases we fix $\gamma = 10$ and $T_1 = 0.2$, while in case b) we fix $\gamma_R = 3T_2/(\gamma\sigma^2)$ with $T_2 = T_1 = 0.2$ and vary Pe by acting on F_a . The inertial, persistence and right residence times therefore are $\tau_I = 0.1$, $\tau_p \sim 16.67$ and $\tau_r^r = 1.65 \cdot 10^3$. The specific choices for T_2 in case a) and F_a in case b) and consequent left well residence times will be instead specified case by case. We evolve the system for time intervals of duration τ , in the following referred to as sampling time, up to $\tau = 3 \cdot 10^4$, the latter in all cases considered resulting much larger than all of the characteristic times of the system.

We sampled the heat per unit time $q = Q/\tau$ for different sampling times τ according to the two definitions Equation 12 and Equation 13 (as in the definitions from subsection 2.2, in the following the subscripts E, W and superscripts L, R will specify case by case which heat in which well is being considered). The heat distributions $p(q)$ are obtained considering $N_p = 10^6$ independent trajectories previously evolved for a time $\tau_{eq} = 10^4$ much larger than all of the characteristic time so as to always start from the stationary configuration. Taking into account that whenever q satisfies a large deviation principle its distributions takes the asymptotic form $p(q) \asymp e^{-\tau I(q)}$, with \asymp asymptotic equivalence symbol underlying sub-exponential contributions $c(q)$ and $I(q)$ rate function [56–58], these distributions are then used to check the validity of the fluctuation theorem Equation 1 by evaluating the ratio

$$\frac{1}{\tau} \log \left(\frac{p(q)}{p(-q)} \right) \asymp I(-q) - I(q) = \left(\frac{1}{T_r} - \frac{1}{T_l} \right) q, \quad (21)$$

where $I(-q) - I(q)$ is the rate function difference appearing in Equation 1 and T_r and T_l denote the temperatures associated to the right and left well, respectively. Note that the symbol \asymp underlies at finite times the appearance of the ratio $(c(q) - c(-q))/\tau$ which become increasingly negligible as time flows. Operatively, the estimates for T_r and T_l , in the following denoted as T_{FT} , are obtained by first evaluating the ratio in the left-hand side of Equation 21 with our numerical distributions $p(q)$ at different τ s and then performing at each of such times a linear fit of the resulting curves. Without loss of generality, in the following we consider settings in which the slope in Equation 21 is positive, corresponding to $T_l > T_r$. While for case a) one intuitively expects T_r (T_l) to coincide with T_1 (T_2) (a circumstance which is indeed verified in subsection 3.1), for case b) we have no a priori indications for the values they could take in presence of the active bath, especially for T_l . In order to extract a T_{FT} estimate for the left well, motivated by the results for case a), we assume $T_r = T_1$, extract $T_{FT} = T_l$ from a fit of

Equation 21 and compare it with the effective and kinetic temperatures T_{eff} and T_{kin} , in turn numerically sampled according to their definitions from Appendix Appendix A.

To conclude, we remark that sampling both positive and negative values of heat becomes increasingly more difficult as the difference between the relevant temperatures of the two baths is made larger. Therefore in the following we implement parameter choices for which such a sampling is numerically feasible.

2.4. Stationary Position Distribution

Before presenting our results, let us comment about the stationary position distribution in the two cases under consideration. These distributions, which we recall can be obtained as the solution of the Fokker-Planck equation with time derivative set to zero [90], provide in fact useful insights on average residence times, in turn useful for our later discussion.

Concerning case a), in the overdamped limit and under the Itô prescription the drift and diffusion coefficients of the Fokker-Planck equation are $-\gamma^{-1}U'(x)$ and $\gamma^{-1}T(x)$ [90,91], respectively, with $T(x)$ x-dependent temperature defined in subsection 2.1. The resulting stationary Fokker-Planck equation has the following solution§

$$p_{st}(x) = \frac{N_I}{T(x)} e^{-\frac{U(x)}{T(x)}} , \quad (22)$$

with N_I normalisation factor and $U(x)$ the quartic potential Equation 2, which is clearly reminiscent of the equilibrium Boltzmann distribution. Note that $p_{st}(x)$ shows a jump discontinuity at x_u when $T_1 \neq T_2$, which disappears when $T_1 = T_2$, i.e. in the usual case of a Brownian particle under the effect of just one equilibrium thermal bath. The associated discontinuity height is $\Delta p_{st} = \left| \lim_{x \uparrow x_u} p_{st}(x) - \lim_{x \downarrow x_u} p_{st}(x) \right| = N_I |T_2^{-1} - T_1^{-1}|$ and becomes more and more marked as the difference $|T_1 - T_2|$ is increased. Note also that the two temperatures T_1 and T_2 determine the shape and height of the distribution in each well, but they play no role in the maxima locations, which in turn come to coincide with the potential minima at $\pm x_m = x_u \pm \sqrt{b/a}$. For the sake of completeness, we mention that under the Stratonovich prescription the diffusion coefficient of the Fokker-Planck equation remains unaltered, while its drift coefficient becomes $\gamma^{-1}(-U'(x) + T(x))$, so that the stationary solution now is

$$p_{st}(x) = N_S e^{-\frac{U(x)}{T(x)}} , \quad (23)$$

with N_S a normalisation factor, which, at variance with Equation 22, is always continuous at x_u also when $T_1 \neq T_2$. We would like to stress that the difference between Equation 22 and Equation 23 can be ultimately traced back to the presence of two regions with different temperatures. In fact, as mentioned in subsection 2.1, in case a)

§ This solution is obtained by first replacing $T(x)$ with a continuous parameter-dependent function $T_\epsilon(x)$ such that $T(x) = \lim_{\epsilon \downarrow 0} T_\epsilon(x)$, then following the standard procedure for the solution of the stationary Fokker-Planck equation with $T_\epsilon(x)$, and finally taking the limit $\epsilon \downarrow 0$.

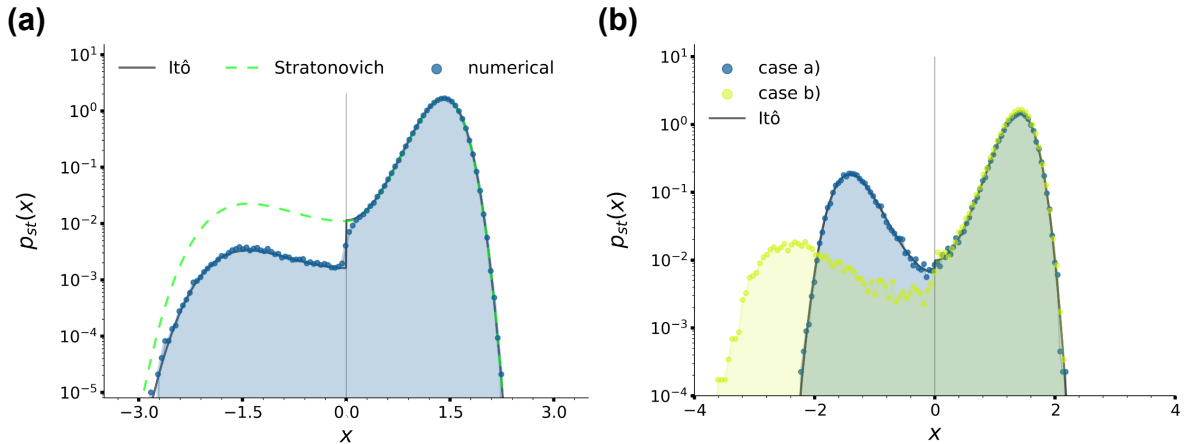


Figure 3. (a): stationary position distributions for case a) with $T_1 = 0.2$ and $T_2 = 1.4$ at sampling time $\tau = 3 \cdot 10^4$. The black solid and green dashed lines are the stationary solutions Equation 22 and Equation 23, respectively, while the blue histogram is the position distribution numerically sampled, as denoted by the legend. (b): stationary position distributions for cases a) and b) and Equation 22, as denoted by the legend. For case a) we fix $T_1 = 0.2$, $T_2 = 0.3$, while for case b) $T_1 = T_2 = 0.2$, $Pe = 50$. In all panels we fixed $\gamma = 10$ and $a = 1.0$, $b = 2.0$.

the Langevin equation Equation 3 can be recast as Equation 6, which is characterized by a multiplicative noise due to the presence of the x -dependent temperature $T(x)$. Therefore, as well known from the literature [90, 92], applying different integration schemes leads to different results, hence the different drift coefficients for the stationary Fokker-Planck equation in the Itô and Stratonovich prescriptions and the resulting different stationary distributions Equation 22 and Equation 23. In Figure 3(a) we provide a comparison between these two stationary solutions and the numerical position distributions at $\tau = 3 \cdot 10^4$ obtained integrating the equations of motions as described in subsection 2.3 setting $T_1 = 0.2$ and $T_2 = 1.4$, so that $|T_1 - T_2| \sim 1$. The figure at the same time shows that the numerical algorithms we use perform integration under the Itô prescription and confirms the presence of the jump discontinuity in Equation 22.

In panel (b) we report instead a comparison between the numerical stationary position distributions for cases a) and b). For case a) we choose $T_1 = 0.2$, $T_2 = 0.3$, while for case b) we fix $T_1 = T_2 = 0.2$ and $F_a = 10$ ($Pe = 50$) so that, as will be shown in subsection 3.2, the kinetic temperature in the left well is $\sim 0.3 = T_2$ (the reason for considering the kinetic temperature will appear clear in subsection 3.2). Note that in the left well for case b) the location $-\tilde{x}_m$ of the peak of the distribution is shifted towards the left with respect to the location of the potential minimum $-x_m$ due to the persistent pushing of the active noise. Even though, up to our knowledge, the stationary Fokker-Planck equation in case b) has no exact analytical solution, our numerical results are coherent with the ones from [74], in which a single active Ornstein-Uhlenbeck particle in a quartic double well potential like Equation 2 is studied. In particular, in [74] the location of the peaks of the distribution are identified as the

points in which the confining force due to the quartic potential Equation 2 and the active force approximated by its average magnitude F_a are balanced, i.e. as the solutions of the equation $-ax^3 + bx = \pm F_a$, where the \pm signs apply to the right and left wells, respectively. In our case, the solution of the above equation relative to the left well gives $-\tilde{x}_m \simeq 2.46$, which is in good agreement with the location of the left peak from panel **(b)**.

To conclude, we point out that the distributions we just commented provide qualitative insights on the average residence time τ_r^r and τ_r^l of the particle in each well, which are essential information especially for case b) in which an analytic estimate for τ_r^l is not available. It is in fact intuitive to see that in general, apart from the specific distribution features, lower temperatures associated to higher peaks in the distributions imply larger residence times, and viceversa for higher temperatures. According to panel **(b)**, we then intuitively expect that the average residence times in the cases under consideration rank as follows: τ_r^r is the largest, τ_r^l in case a) is intermediate and finally τ_r^l in case b) is the shortest.

3. Results

3.1. Heat Exchanges between Two Passive Baths

We start in this section with the investigation of case a) envisaging a passive bath in each of the two wells. We first fix $T_1 = 0.2$ and consider three T_2 values, 0.22, 0.3 and 0.4. According to Equation 11, the corresponding average residence times τ_r^l are much larger than the inertial time $t_I = 0.1$, ranging from $\tau_r^l = 1.05 \cdot 10^3$ for $T_2 = 0.22$ to $\tau_r^l = 1.35 \cdot 10^2$ for $T_2 = 0.4$. In Figure 4**(a)** we show the distribution $p(q_E^R)$ for these three choices of temperatures at sampling time $\tau = 3 \cdot 10^4$ (the distributions $p(q_E^L)$ are just symmetrical). Note that all distributions are characterised by a positive average value, $\sim 2.10 \cdot 10^{-5}$ for $T_2 = 0.22$, $\sim 1.34 \cdot 10^{-4}$ for $T_2 = 0.3$ and $\sim 2.68 \cdot 10^{-4}$ for $T_2 = 0.4$, confirming that, as intuitively expected, on average the colder bath in the right well receives more energy from the hotter bath in the left well than the one it outputs towards it through the jumping particle. Note also that the distributions are characterised by an increasing skewness as the temperature difference $\Delta T = |T_1 - T_2|$ is increased. In the remainder of the present section we focus on the case $T_1 = 0.2$, $T_2 = 0.3$, which at the same time guarantees an appreciable skewness of $p(q_E^R)$ as well as an efficient sampling of both positive and negative heat values. Up to what our simulations afforded us to sample, we checked that the results we are about to discuss for this case also apply to the other values of T_2 .

In order to study the validity of Equation 1, we first focus on the trend of $-\ln(p(q_E^R))/\tau$, which in the large time limit converges to the rate function $I(q_E^R)$ whenever q_E^R satisfies a large deviation principle [56–58]. More specifically, in Figure 4**(b)** we report $-\ln(p(q_E^R)/A_\tau)/\tau$ extracted at different sampling time τ s, as reported by the legend. At each sampling time, A_τ denotes the maximum of the distribution and in the

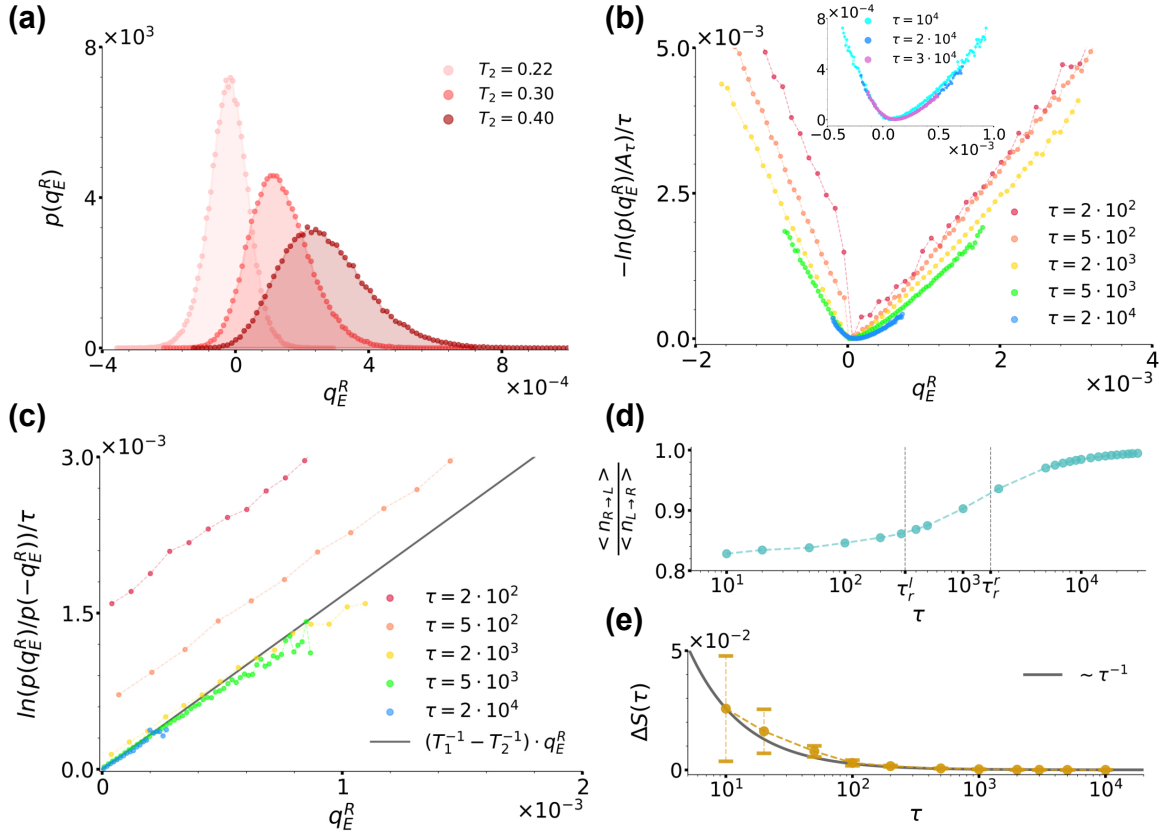


Figure 4. (a): distribution $p(q_E^R)$ for case a) at sampling time $\tau = 3 \cdot 10^4$ for $T_2 = 0.22$, 0.3 and 0.4 , as denoted by the legend. (b): curves $-\ln(p(q_E^R)/A_\tau)/\tau$ for $T_2 = 0.3$ at different sampling times, as denoted by the legend. A_τ denotes the maximum of the distribution at each sampling time. The inset shows instead the trend of the same curves at the largest sampling times considered. (c): ratio $\ln(p(q_E^R)/p(-q_E^R))/\tau$ evaluated at different sampling times τ using data from panel (b) along with the right hand-side of Equation 21 plotted with $T_r = T_l = 0.2$ and $T_l = T_2 = 0.3$, as denoted by the legend. (d): ratio between the average number of jumps in the right \rightarrow left direction and left \rightarrow right directions denoted $\langle n_{R \rightarrow L} \rangle$ and $\langle n_{L \rightarrow R} \rangle$, respectively, as a function of sampling time. The dashed lines denote the left and right average residence times $\tau_r^l = 3.11 \cdot 10^2$ and $\tau_r^r = 1.64 \cdot 10^3$, respectively. (e): shift $\Delta S(\tau)$ of the curves from panel (c) as a function of time. For comparison, here the black solid line reports the trend of $\sim \tau^{-1}$. In all panels we fixed $\gamma = 10$, $T_1 = 0.2$ and $a = 1.0$, $b = 2.0$.

ratio it makes the resulting curves shift vertically so as to have a minimum value of zero. As highlighted by the inset of Figure 4(b), for $\tau > 10^4 \gg \tau_l = 0.1$ we observe that the curves do overlap, thus implying q_E^R to satisfy a large deviation principle. We therefore proceed to check the validity of Equation 1 as prescribed by Equation 21. We use data from Figure 4(b) and report the resulting curves at the same τ s in Figure 4(c), as denoted by the legend. We find that at all τ s these curves are linear and, within numerical error, with slope in agreement with $1/T_1 - 1/T_2$, so that we can identify T_r with T_1 and T_l with T_2 . We would like to underline that while previous results proved a

fluctuation theorem like Equation 1 to stand in the case of two different thermal baths separately at equilibrium but acting simultaneously everywhere in the system [55, 59, 60], our results extend this scenario to the case of spatially separated baths.

Interestingly, Figure 4(c) also shows that at short times the numerical lines in Figure 4(c) do not cross the origin, but rather present a time-decreasing positive shift $\Delta S(\tau)$ which we can explain by looking at the system phenomenology at short times. During the evolution of our system, three timescales come into play, i.e. the left and right well residence times, $\tau_r^l \simeq 3.11 \cdot 10^2 < \tau_r^r \simeq 1.64 \cdot 10^3$, and the sampling time τ at which the distribution $p(q_E^R)$ is considered. When taking into account a large number N_p independent realizations of the system, one then intuitively expects that, as long as $\tau < \tau_r^r$, more jumps from left to right occur than in the opposite direction, while when $\tau_r^l < \tau < \tau_r^r$, the number of right \rightarrow left jumps starts increasing until essentially matching the number of left \rightarrow right ones at $\tau \gg \tau_r^l, \tau_r^r$. Figure 4(d) confirms this intuition by showing the trend of the numerical ratio between the average number of jumps in the right \rightarrow left and in the left \rightarrow right directions, respectively denoted as $\langle n_{R \rightarrow L} \rangle$ and $\langle n_{L \rightarrow R} \rangle$, as a function of sampling time τ . The curve in fact starts from a value lower than one for $\tau < \tau_r^l$, which then it reaches asymptotically from below when $\tau \gg \tau_r^r$. This jumps phenomenology clearly bears consequences on the distribution $p(q_E^R)$, and then on the resulting fluctuation theorem. In fact, as apparent from Figure 4(b), at short times $\tau < \tau_r^l$ its left and right branches weigh differently positive and negative heat values, the left branch being further away from its large-time stationary form than the right one and mirroring the jump imbalance biased towards left \rightarrow right positive heat jumps. As mentioned in subsection 2.3 when commenting Equation 21, these effects are encoded in the distribution as a sub-exponential contribution $c(q_E^R)$, which is a function of q_E^R scaling as t^α with $\alpha < 1$ and in our case is directly related with the observed shift $\Delta S(\tau)$. As shown in Figure 4(e), we in fact find $\Delta S(\tau) = (c(q_E^R) - c(-q_E^R))/\tau$ to decrease as $\simeq \tau^{-1}$ corresponding to $\alpha \simeq 0$, the latter value signalling that the difference $c(q_E^R) - c(-q_E^R)$ is of order $\sim \mathcal{O}(1)$.

We now discuss the validity of the fluctuation theorem from Equation 1 for q_W^R by studying $p(q_W^R)$ by comparison with $p(q_E^R)$. In Figure 5(a) and (b) we compare the distributions $p(q_W^R)$ and $p(q_E^R)$ for the same parameter choice as in Figure 4(b) at sampling times $\tau = 10^3$ and $\tau = 3 \cdot 10^4$, respectively. Let us focus on Figure 5(a) first. What immediately catches the eye is that, at variance with $p(q_E^R)$ and as highlighted by the vertical arrows, $p(q_W^R)$ is characterized by three peaks. This peculiar structure can be readily explained by recalling the jump phenomenology discussed above. The left and right external peaks highlighted by the red arrows are due to particles leaving and entering the right well, which are then responsible for negative and positive energy exchanges, respectively. As here $\tau_r^l < \tau < \tau_r^r$, more particles have jumped from left to right than in the opposite direction, hence the higher right peak. However, in our large sample of N_p independent realizations, at this time a large number of particle has not yet jumped at all from the right well, but rather have been exchanging an average zero heat with the equilibrium thermal bath in this well, hence the central peak located at $q_W^R = 0$

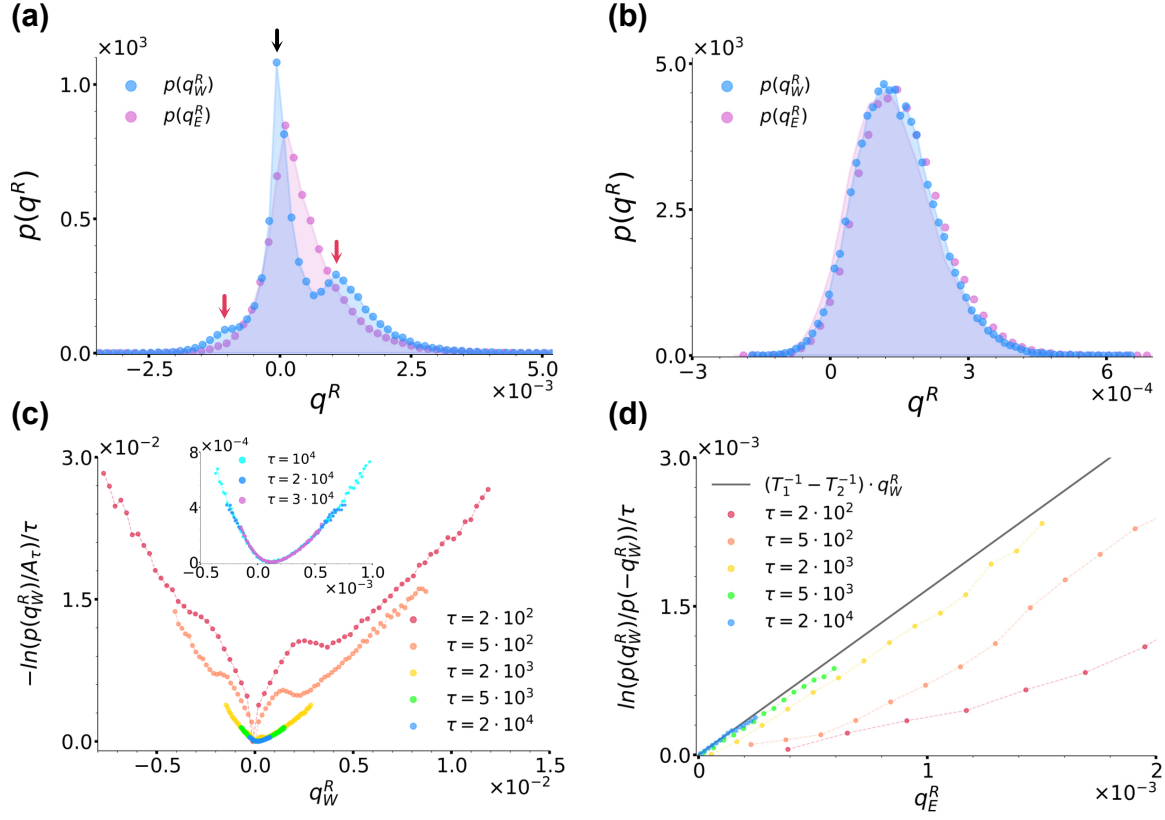


Figure 5. (a) and (b): comparison between the distributions $p(q_E^R)$ and $p(q_W^R)$ at sampling times $\tau = 10^3$ and $\tau = 3 \cdot 10^4$, respectively, with same parameters as in Figure 4. In panel (a) the three arrows highlight the three peaks of $p(q_W^R)$. (c): curves $-\ln(p(q_W^R)/A_\tau)/\tau$ for $T_2 = 0.3$ at different sampling times, as denoted by the legend. As in Figure 4, A_τ denotes the maximum of the distribution at each sampling time. The inset shows instead the trend of the same curves at the largest sampling times considered. (d): ratio $\ln(p(q_W^R)/p(-q_W^R))/\tau$ evaluated at different sampling times using data from panel (c) along with the right hand-side of Equation 21 plotted with $T_r = T_1 = 0.2$ and $T_l = T_2 = 0.3$, as denoted by the legend. In all panels we fixed $\gamma = 10$, $T_1 = 0.2$ and $a = 1.0$, $b = 2.0$.

highlighted by the black arrow. At large times, $p(q_W^R)$ instead loses its three-peaks structure and comes to coincide with $p(q_E^R)$ from Figure 4(b). In particular, the central peak disappears because at large times it is extremely probable that all particles have already jumped almost once, while the other two get closer and closer until eventually merging. This overall scenario is graphically confirmed and clarified by Figure 5(c), which reports the curves $-\ln(p(q_W^R)/A_\tau)/\tau$ extracted at different sampling times τ s, as denoted by the legend. The figure in fact at the same time shows the two external peaks clearly getting closer until eventually merging and also the curves converging towards a convex rate function $I(q_W^R)$. Combining further this last information with the content of Figure 4(b) and Figure 5(b), we can therefore affirm that at large times $I(q_W^R) = I(q_E^R)$. The curves from Figure 5(c) allow us to finally check the validity of a

fluctuation theorem for q_W^R as prescribed by Equation 21. Figure 5(d) reports the ratio $\ln(p(q_W^R)/p(-q_W^R))/\tau$ evaluated at different sampling times using data from panel (c) and, as highlighted by the black line reporting Equation 21 plotted with $T_r = T_1 = 0.2$ and $T_l = T_2 = 0.3$, shows that at large sampling time τ q_W^R indeed satisfies the same fluctuation theorem shown in Figure 4(c) to be satisfied by q_E^R with same slope. Note that at short times the fluctuation theorem is not satisfied because of the sub-exponential contribution $(c(q_W^R) - c(-q_W^R))/\tau$ which encodes the three-peaks structure of $p(q_W^R)$ and makes the curve actually curvilinear rather than rigidly vertically shifted. To conclude we report that for the left well we checked that $p(q_W^L) = p(-q_W^R)$ and consequently that the same results discussed until this point for q_W^R symmetrically still apply so that the energy balance Equation 19 results satisfied.

3.2. Heat Exchanges between a Passive and an Active Bath

In this section we investigate case b) envisaging a left bath which is given an active character through the introduction of an additional Ornstein-Uhlenbeck noise. In Figure 6(a) we preliminarily show the distribution $p(q_E^R)$ for $T_1 = T_2 = 0.2$ and three different Pe at sampling time $\tau = 3 \cdot 10^4$ (the distributions $p(q_W^R)$ are just symmetrical). The figure is clearly reminiscent of Figure 4(a), with Pe effectively playing the role of a temperature like T_2 : as Pe is increased, the distributions shift towards the right, with a consequent increase of their skewness as well as of the average value of q_E^R .

Let us consider in detail the case $Pe = 50.0$. As in subsection 3.1, for the right well the residence time is $\tau_r^r \sim 1.64 \cdot 10^3$ as prescribed by Equation 11. For the left well we instead numerically estimate it as $\tau_r^l \sim 34.18$, so that the conditions $\tau_r^l, \tau_r^r > \tau_p = 16.67 \gg \tau_l = 0.1$ are satisfied. Figure 6(b) shows the trend of $-\ln(p(q_E^R))/\tau$ for increasing sampling time τ , as denoted by the legend. As remarked by the inset and similarly to subsection 3.1, also in this case we find the curves to converge at large times towards a convex rate function $I(q_E^R)$, thus proving q_E^R to satisfy a large deviation principle even when one of the baths is made active. Figure 6(c) shows instead the ratio $\ln(p(q_E^R)/p(-q_E^R))/\tau$ evaluated at different times using data from Figure 6(b). Interestingly, also in this case the resulting curves show a linear trend at all times. Here the effect of the sub-exponential contribution $c(q_E^R)$ makes the slope of the curves reduce until reaching a constant value, as remarked by the inset. Following the same line of action as in subsection 3.1, one can fit these lines as prescribed by Equation 21 so as to extract a temperature estimate for the right well based on fluctuation theorems. When doing so identifying a priori T_r with $T_1 = 0.2$, one finds for the left well $T_{FT}^{q_E^R} \sim 0.3$ (whence the choice of parameters in Figure 3(b) for which $T_2 = 0.3$ from case a) and $T_{FT}^{q_E^R} \sim 0.3$ from case b) essentially coincide). The resulting line $(T_1^{-1} - (T_{FT}^{q_E^R})^{-1}) \cdot q_E^R$ is reported in Figure 6(c) for completeness. The possibility $T_l = T_2 = 0.2$ can thus be trivially discarded as, like in the case $Pe = 5$ from Figure 6(a) in which the effect of the active noise is essentially negligible, it would lead to $p(q_E) = p(-q_E)$, and therefore to a vanishing slope.

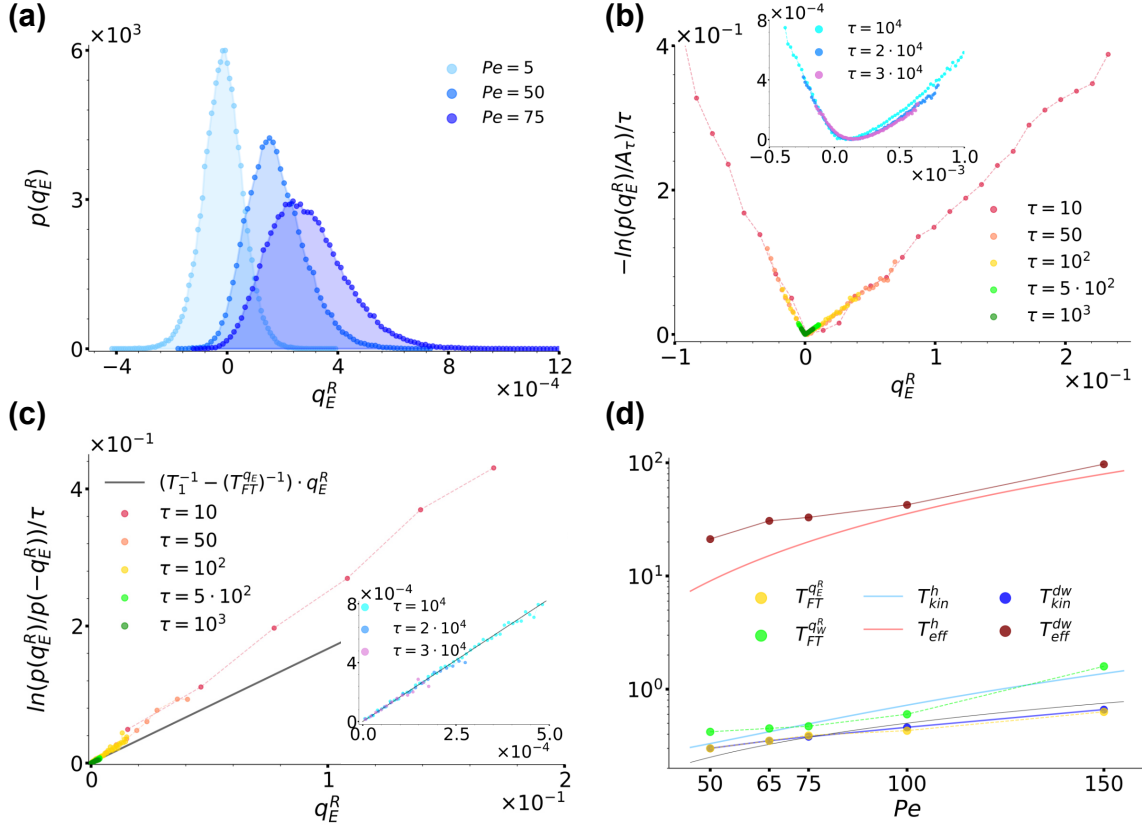


Figure 6. (a): distribution $p(q_E^R)$ for case b) at sampling time $\tau = 3 \cdot 10^4$ for $Pe = 5, 50$ and 75 , as denoted by the legend. (b): curves $-\ln(p(q_E^R)/A_\tau)/\tau$ for $Pe = 50$ at different sampling times, as denoted by the legend. As in Figure 4, A_τ still denotes the maximum of the distribution at each sampling time. The inset shows instead the trend of the same curves at the largest sampling times considered. (c): ratio $\ln(p(q_E^R)/p(-q_E^R))/\tau$ evaluated at different sampling times τ up to $\tau = 10^3$ in the main figure and between $\tau = 10^4$ and $\tau = 3 \cdot 10^4$ in the inset, as denoted by legends. Main and inset were obtained using data from main and inset of panel (b), respectively, and both report the trend of $(T_1^{-1} - T_{FT}^{-1}) \cdot q_E$ as a black solid line, with $T_{FT} \sim 0.3$ extracted from a fit of the curves in the inset performed as described in the main text. (d): overview of the temperatures $T_{FT}^{q_E^R}$ and $T_{FT}^{q_W^R}$ (yellow and green circles) extracted from $p(q_E^R)$ and $p(q_W^R)$ at sampling time $\tau = 3 \cdot 10^4$ as prescribed by Equation 21 as a function of Pe compared to T_{kin}^h, T_{eff}^h and $T_{kin}^{dw}, T_{eff}^{dw}$ obtained in the harmonic (light blue and red lines) and double-well (dark blue and red lines) configurations, respectively. T_{kin}^h and T_{eff}^h are plotted as solid lines to highlight their analytical origin from Equation A.12 and Equation A.13, while all other data are plotted as dot and lines, the dots reporting the values obtained numerically, the lines being a guide to the eye, including the lower black solid line reporting a sample linear trend $\sim Pe$. In all panels we fixed $\gamma = 10$ and $T_1 = T_2 = 0.2$, while in the harmonic and double-well configurations we set $k = 4.0$ and $a = 1.0, b = 2.0$, respectively.

At this point one could naturally ask how $T_{FT}^{q_E^R}$ is influenced by the strength of the activity, i.e. by Pe , and also whether this temperature does coincide with other out-of-equilibrium temperatures like the kinetic and effective ones mentioned in section 1

| Pe | τ_r^l | $T_{FT}^{qE^R}$ | $T_{FT}^{qW^R}$ | T_{eff}^h | T_{kin}^h | T_{eff}^{dw} | T_{kin}^{dw} |
|-------|------------|-----------------|-----------------|-------------|-------------|----------------|----------------|
| 50.0 | 34.18 | 0.30 | 0.42 | 22.05 | 0.33 | 21.20 | 0.30 |
| 65.0 | 32.09 | 0.35 | 0.45 | 37.13 | 0.42 | 30.68 | 0.35 |
| 75.0 | 31.41 | 0.39 | 0.47 | 49.36 | 0.49 | 32.92 | 0.38 |
| 100.0 | 29.85 | 0.43 | 0.60 | 92.42 | 0.72 | 37.49 | 0.46 |
| 150.0 | 27.36 | 0.63 | 1.59 | 207.69 | 1.43 | 97.12 | 0.66 |

Table 1. Estimates of the average residence time in the left well τ_r^l and of the temperatures T_{qE^R} , T_{qW^R} , T_{eff}^h , T_{kin}^h , T_{eff}^{dw} , T_{kin}^{dw} for various choices of increasing Pe . The values of T_{eff}^h , T_{kin}^h are obtained analytically from Equation A.12 and Equation A.13, while all other time and temperature estimates are obtained numerically. In all cases the system was evolved until $\tau = 3 \cdot 10^4$ and we fixed $\gamma = 10$ and $T_1 = 0.2$, $T_2 = 0.2$, while in the harmonic and double-well configurations we set $k = 4.0$ and $a = 1.0$, $b = 2.0$, respectively.

and detailed in Appendix Appendix A. Concerning the first question, Figure 6(d) shows the trend of $T_{FT}^{qE^R}$ (yellow dots) obtained varying Pe while keeping fixed all other system parameters, while Table 1 reports the exact values emerged from the analytical expressions from Appendix Appendix A and from our fit procedure performed keeping $T_r = T_1 = 0.2$ fixed. The data suggest that $T_{FT}^{qE^R}$ increases roughly linearly as a function of Pe . Note that at all Pe considered the estimated left residence times τ_r^l satisfy the condition $\tau_r^l > \tau_p = 16.67 \gg \tau_I = 0.1$, as reported in Table 1.

In order to answer the second question, we instead compare $T_{FT}^{qE^R}$ with the kinetic and effective temperatures obtained for a particle subjected everywhere to the active bath and under the separate action of two different external potentials. The first potential we consider is a harmonic one $U(x) = kx^2/2$ introduced in such a way to approximate the quartic double well Equation 2 around one of its minima, i.e setting setting $k = 2b$ with $2b$ second derivative of Equation 2 at its minima locations $\pm x_m$. In such a case we refer to the overall configuration as harmonic configuration, the two temperatures are denoted as T_{eff}^h and T_{kin}^h and, as detailed in Appendix Appendix A, an analytical derivation is feasible with resulting expressions provided by Equation A.12 and Equation A.13. The second potential we consider is instead the usual quartic double well potential Equation 2, and the relative configuration is referred to as double-well configuration. Here the two temperatures are denoted T_{eff}^{dw} and T_{kin}^{dw} and their estimates are obtained by numerical means. The rationale underlying these configurations follows our desire to understand if the value of $T_{FT}^{qE^R}$ is determined mostly by the permanence of the particle around the potential minimum (hence the harmonic configuration), or, similarly to what observed for the variation of the entropy production for an active particle under the action of a quartic double-well potential [74,93], by the non-convex region of Equation 2 (hence the double-well configuration).

Figure 6(d) reports the trend of the temperature values we obtained in the two configurations under consideration, while Table 1 offers an overview of their values. From

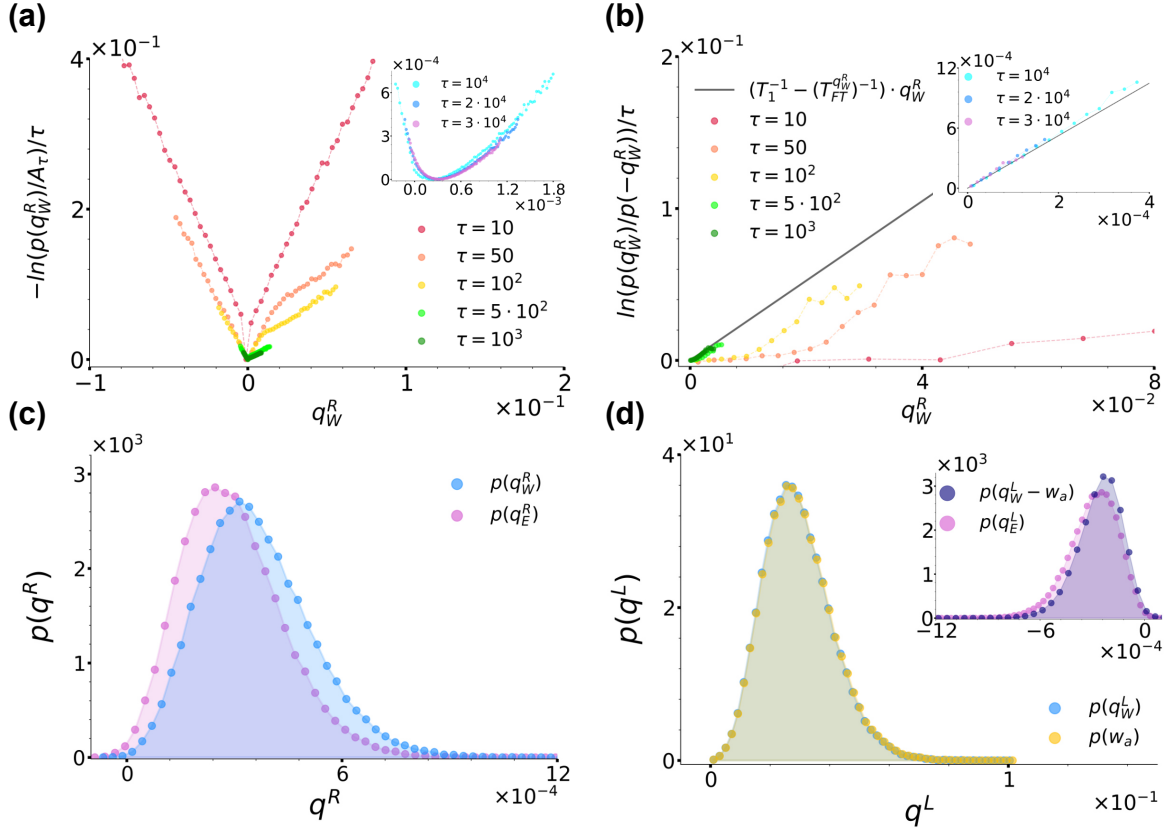


Figure 7. (a): curves $-\ln(p(q_W^R))/\tau$ for $Pe = 50$ at different sampling times, as denoted by the legend. A_τ denotes the maximum of the distribution at each sampling time. The inset shows instead the trend of the same curves at the largest sampling times considered. (b): ratio $\ln(p(q_W^R)/p(-q_W^R))/\tau$ evaluated at different sampling times using data from panel (a) along with the right hand-side of Equation 21 with $T_r = 0.2$ fixed and $T_l = T_{FT}^{q_W^R} \sim 0.42$ extracted from a fit of the curves in the inset performed as described in the main text, as denoted by the legend. (c) and (d): comparison between the distributions $p(q_E^R)$, $p(q_W^R)$ and $p(q_W^L)$, $p(w_a)$ at sampling time $\tau = 3 \cdot 10^4$, respectively, with same parameters as in Figure 6(a). In panel (d) the inset shows instead a comparison between $p(q_E^L)$ and $p(q_W^L - w_a)$. In all panels we fixed $\gamma = 10$, $T_1 = T_2 = 0.2$ and $a = 1.0$, $b = 2.0$.

a comparison with the trends and values of $T_{FT}^{q_E^R}$ it is immediate to realise that there is no correspondence between any of the two effective temperatures. The kinetic temperature is instead much closer to $T_{FT}^{q_E^R}$, with T_{kin}^{dw} essentially coinciding exactly. We therefore conclude that it is not enough to limit our attention to the evolution of the particle around the potential minima, but rather considering its dynamics around its local maximum at x_u is essential. Moreover, the affinity of $T_{FT}^{q_E^R}$ to the kinetic temperature seems to mirror the inherent character of \mathcal{Q}_E^R : instantaneous energy exchanges are best described in terms of an instantaneous out-of-equilibrium temperature.

We now turn to comment on the behaviour of the heat q_W and active work w_a per unit time. Figure 7(a) reports the curves $-\ln(p(q_W^R))/\tau$ for increasing sampling time

τ for the same parameter choice as in Figure 6(b). Along with its inset, the figure shows that also in this case these curves converge at large times towards a convex rate function $I(q_W^R)$, thus proving q_W^R to satisfy a large deviation principle also when the left bath is active. Concerning the validity of a fluctuation theorem, Figure 7(b) shows the ratio $\ln(p(q_W^R)/p(-q_W^R))/\tau$ evaluated at different times using data from Figure 7(a). As in Figure 5(d), at small times the sub-exponential contribution $(c(q_W^R) - c(-q_W^R))/\tau$ makes the resulting curves actually curvilinear, while at large times they assume a linear trend with constant slope. Following the usual fitting procedure, in this case we find $T_{FT}^{q_W^R} \sim 0.42$, and the resulting curve $(T_1^{-1} - (T_{FT}^{q_W^R})^{-1}) \cdot q_W^R$ is reported in Figure 7(b) and its inset for completeness. In order to give context to this finding, Figure 7(c) reports a comparison between $p(q_W^R)$ and $p(q_E^R)$ at sampling time $\tau = 3 \cdot 10^4$. Interestingly, at variance with Figure 5(b) from case a), here at large times the two distributions do not coincide, but rather $p(q_W^R)$ results slightly shifted towards the right with respect to $p(q_E^R)$. As Figure 6(b) and Figure 7(a) show that at this τ the curves $-\ln(p(q_E^R))/\tau$ and $-\ln(p(q_W^R))/\tau$ have both already converged towards their respective rate functions, the origin of this discrepancy is not a matter of not long enough sampling time, but its explanation must rather be searched once again in the very dynamics of the system. To this end, we reconsider the position stationary distribution from Figure 3(b). As commented in subsection 2.4, this is characterized by a left peak shifted towards the left with respect to the location of the left minimum $-x_m$ of the double-well potential Equation 2. This effect is in turn ascribable to the action of the active noise $a(t)$ which pushes the particle towards the left when assuming persistently negative values. When instead $a(t)$ persistently assumes positive values, it pushes the particle towards the right until making it jump in the right well. In doing so, the particle essentially takes a run-up, so that, at variance with case a), when jumping towards the right its velocity is enhanced. As a consequence the particle is not able to dissipate all accumulated excess energy essentially instantaneously at x_u as in case a), but rather it completes its thermalization with the right well bath during the descent towards the right minimum located at x_m , hence the released surplus energy, the shift of $p(q_W^R)$ and the resulting fit temperature $T_{FT}^{q_W^R}$ higher than both $T_{FT}^{q_E^R}, T_{kin}^{dw} \sim 0.3$.

We remark that this finding is coherent with the phenomenology described above: the release of energy associated to q_W^R does not occur instantaneously so the kinetic temperature is obviously not fit to describe this phenomenon. At the same this energy release does not persist long enough to make the effective temperature $T_{eff}^{dw} \sim 21.2$ intervene, so that $T_{kin}^{dw} \sim T_{FT}^{q_E^R} < T_{FT}^{q_W^R} < T_{eff}^{dw}$. Interestingly, Figure 6(d) and Table 1 show that the temperature discrepancies we uncovered at $Pe = 50$ are not peculiar of this specific case, but instead are common for all other Pe we considered, with $T_{kin}^{dw} \sim T_{FT}^{q_E^R} < T_{FT}^{q_W^R} < T_{eff}^{dw}$ in all cases.

To conclude, we briefly comment on the heat exchanges distributions for the left bath, captured at sampling time $\tau = 3 \cdot 10^4$ and $Pe = 50$. Figure 7(d) reports $p(q_W^L)$ and $p(w_a)$ and shows that values spanned by these distributions are much larger than the

ones spanned by $p(q_W^R)$ and $p(q_E^R)$ from Figure 7(c). This effect is due to the enhanced velocity of the particle pushed by the active force. Note also that the signs of q_W^L and w_a agree and their distributions almost overlap. That they do not completely overlap is in turn shown by the inset reporting $p(q_W^L - w_a)$ compared to $p(q_E^L) = p(-q_E^R)$. The inset in fact shows that $p(q_W^L - w_a)$ records non-zero values of three orders of magnitude lower than those associated to the distributions from the main figure and of the same order of magnitude as the ones associated to $p(q_E^L)$. Moreover, similarly to what happens for $p(q_W^R)$ and $p(q_E^R)$ from Figure 7(c), $p(q_W^L - w_a)$ is slightly shifted with respect to $p(q_E^L)$. Finally, we conclude by remarking that the distributions $p(q_W^R)$ and $p(q_W^L - w_a)$ result coherent with the energy balance Equation 19.

4. Conclusions

In this paper we numerically studied the heat exchanges occurring between two heat baths of different nature with the purpose to investigate on the role temperature plays in these phenomena. The baths were spatially confined in the two wells of a quartic double well potential, while the heat exchanges were mediated by a Brownian particle jumping between the two. Heat was sampled according to two different definitions: as the total kinetic energy carried by the particle when jump events occur and as the work performed by the particle on one of the two baths when immersed in it. The distributions of these heats were used to check the validity of a fluctuation theorem whence possibly extracting a temperature estimate for the baths through a proper linear fit. This procedure allowed us to introduce the definition of an out-of-equilibrium temperature whose resulting values we compared not only with the bath temperatures, but also with other out-of-equilibrium temperatures as the kinetic and effective ones. Operatively, we fixed an equilibrium bath in the right well and considered two different configurations for the one in the left well.

In the first case we fixed another equilibrium thermal bath with a different temperature and found both heats definitions to satisfy the same fluctuation theorem with fit temperatures coinciding with the ones of the two baths. These results extend the analysis of [55, 59, 60] to the cases of spatially separated equilibrium thermal baths.

In the second case we instead considered an active bath by introducing an additional Ornstein-Uhlenbeck noise, making the bath effectively out of equilibrium. Also in this case we found a fluctuation theorem to be satisfied. However, here the temperature relative to the left bath turns out to coincide with its out-of-equilibrium kinetic temperature for the heat defined as sum of kinetic energies and with a higher one still lower than the effective temperature for the other definition of heat. These results and discrepancies were interpreted by looking at the system phenomenology, finding them to mirror the instantaneous or longer release of energy captured by the two heat definitions.

The present study could represent the first step towards a deeper and wider investigation on the role played by temperature in heat exchanges. If and where

possible, analytical approaches could in fact provide further validation and insights to the overall scenario emerged from our investigation. Moreover more complex geometries and bath features could be explored so as to clarify even better the role of kinetic temperature in heat exchanges or reveal cases where instead the effective temperature plays a prominent role. Experiments adopting setups and technologies already in place like Janus particles [76–79] and optical tweezers [80,81] could provide further validation and connections with real systems.

Appendix A. Effective and Kinetic temperature

Effective and *kinetic* temperatures are two out of equilibrium temperature definitions able to capture instantaneous and time-delayed properties of the system [3,4,46,48,61–66], respectively. Their definitions rely in fact on two fundamental results of statistical mechanics more effective in these two time regimes: the equipartition theorem [94] and the fluctuation-dissipation theorem [95].

Concerning the effective temperature, we first recall the definition of mean square displacement and integrated linear response function. The former is defined as

$$\Delta^2(t', t) \equiv \langle [\mathbf{r}(t) - \mathbf{r}(t')]^2 \rangle , \quad (\text{A.1})$$

and measures how far on average a particle travels over time with respect to a fixed initial location, while the latter is defined as

$$\chi(t', t) \equiv \int_{t'}^t dt'' \sum_{\alpha=1}^d R_{\alpha\alpha}(t'', t) , \quad (\text{A.2})$$

with

$$R_{\alpha\beta}(t', t) = \left. \frac{\delta \langle r_\alpha(t) \rangle_h^\lambda}{\delta h_\beta^\lambda(t')} \right|_{h_\beta^\lambda=0} \quad (\text{A.3})$$

linear response of the system, d dimension of the system, α, β dimensional indices and $h_\beta^\lambda(t')$ an external perturbation depending on the parameter λ and measures how a system responds to a small external perturbation. The above two functions are both involved in the position fluctuation-dissipation theorem

$$2T\chi(t', t) = \Delta^2(t', t) . \quad (\text{A.4})$$

Based on the above relation, the time dependent effective temperature for an out-of-equilibrium systems is then defined as [3,4,65]

$$T_{eff}(t', t) \equiv \frac{\Delta^2(t', t)}{2\chi(t', t)} . \quad (\text{A.5})$$

Concerning the kinetic temperature, we recall the equipartition theorem to state that for each degree of freedom i of an equilibrium system, the temperature T and the velocity fluctuations are related as

$$\frac{1}{2}m \langle \dot{\mathbf{r}}_i^2(t) \rangle = \frac{1}{2}k_B T . \quad (\text{A.6})$$

It is then natural for each degree of freedom of an out-of-equilibrium system to define the time-dependent kinetic temperature as [4, 48, 66]

$$T_{kin}(t) \equiv \frac{m \langle \dot{\mathbf{r}}_i^2(t) \rangle}{k_B}. \quad (\text{A.7})$$

In equilibrium systems, as for example a single brownian particle in contact with a white-noise bath with temperature T , the two definitions boil down to the same expression, T . In more complex configurations they can instead be very different. For example, for a free active Ornstein-Uhlenbeck particle [67–70], i.e. a particular instance of active particle, the integrated linear response function reads

$$\chi(t', t) = \frac{t - t'}{\gamma}, \quad (\text{A.8})$$

while the mean square displacement and velocity expressions are provided by [68]. Combining these functions as prescribed by Equation A.5 and Equation A.7 and fixing $t' = 0$ one finds that in the long time limit $t \uparrow \infty$

$$T_{eff} \longrightarrow T + \frac{F_a^2}{\gamma\gamma_R}. \quad (\text{A.9})$$

and

$$T_{kin} \longrightarrow T + \frac{F_a^2}{\gamma} \frac{1}{(\gamma_R + \frac{\gamma}{m})}, \quad (\text{A.10})$$

where we dropped the time dependence as both temperatures reach a constant value. Analytical estimates can also be provided for an active Ornstein-Uhlenbeck particle under the action of an external harmonic potential like $U(x) = kx^2/2$. In this case the integrated linear response function is

$$\chi(t', t) = \frac{1 - e^{-\frac{\gamma}{k}(t-t')}}{k}, \quad (\text{A.11})$$

while the mean and velocity square displacement expressions are again provided by [68]. Combining these functions as above and fixing $t' = 0$ one finds that in the long time limit $t \uparrow \infty$

$$T_{eff} \longrightarrow T + \frac{F_a^2}{\gamma} \frac{1 + \frac{\gamma}{m\gamma_R}}{(\gamma_R + \frac{\gamma}{m} + \frac{k}{m\gamma_R})}. \quad (\text{A.12})$$

and

$$T_{kin} \longrightarrow T + \frac{F_a^2}{\gamma} \frac{1}{(\gamma_R + \frac{\gamma}{m} + \frac{k}{m\gamma_R})} \quad (\text{A.13})$$

which in the limit $k \downarrow 0$ reduce to Equation A.9 and Equation A.10, respectively.

Up to our knowledge, in even more complex systems, analytical results are not available. However, one can always resort to numerical methods and evaluate the kinetic and effective temperatures as prescribed by their definitions Equation A.5 and Equation A.7. In particular, the effective temperature estimation requires the knowledge of the integrated linear response function, to be evaluated using an external perturbation low enough for the system to remain in the linear regime and at the same time large enough to overcome large fluctuation effects.

References

- [1] Cugliandolo L F, Kurchan J and Peliti L 1997 *Phys. Rev. E* **55**(4) 3898–3914 URL <https://link.aps.org/doi/10.1103/PhysRevE.55.3898>
- [2] Cugliandolo L F and Kurchan J 2000 *Journal of the Physical Society of Japan - Supplement A* **69**(247)
- [3] Cugliandolo L F 2011 *Journal of Physics A: Mathematical and Theoretical* **44** 483001 URL <https://doi.org/10.1088/1751-8113/44/48/483001>
- [4] Ilg P and Barrat J L 2006 *Journal of Physics: Conference Series* **40** 76–85 URL <https://doi.org/10.1088/1742-6596/40/1/009>
- [5] Ramaswamy S 2010 *Annu. Rev. Condens. Matter Phys.* **1** 323–345 URL <https://doi.org/10.1146/annurev-conmatphys-070909-104101>
- [6] Romanczuk P, Bär M, Ebeling W, Lindner B and Schimansky-Geier L 2012 *The European Physical Journal Special Topics* **202** 1–162 URL <https://doi.org/10.1140/epjst/e2012-01529-y>
- [7] Marchetti M C, Joanny J F, Ramaswamy S, Liverpool T B, Prost J, Rao M and Simha R A 2013 *Rev. Mod. Phys.* **85**(3) 1143–1189 URL <https://link.aps.org/doi/10.1103/RevModPhys.85.1143>
- [8] Elgeti J, Winkler R G and Gompper G 2015 *Reports on progress in physics* **78** 056601 URL <https://dx.doi.org/10.1088/0034-4885/78/5/056601>
- [9] Bechinger C, Di Leonardo R, Löwen H, Reichhardt C, Volpe G and Volpe G 2016 *Reviews of Modern Physics* **88** 045006 URL <https://doi.org/10.1103/RevModPhys.88.045006>
- [10] Fodor E and Marchetti M C 2018 *Physica A: Statistical Mechanics and its Applications* **504** 106–120 ISSN 0378-4371 lecture Notes of the 14th International Summer School on Fundamental Problems in Statistical Physics URL <https://www.sciencedirect.com/science/article/pii/S0378437117313869>
- [11] Carenza L N, Gonnella G, Lamura A and Negro G 2019 *International Journal of Modern Physics C* **30** 1941002 URL <https://doi.org/10.1142/S012918311941002X>
- [12] Negro G, Lamura A, Gonnella G and Marenduzzo D 2019 *Europhysics Letters* **127** 58001
- [13] Gompper G *et al.* 2020 *J. Phys. Condens. Matter* **32** 193001 URL <https://doi.org/10.1088/1361-648x/ab6348>
- [14] Carenza L, Gonnella G, Lamura A, Marenduzzo D, Negro G and Tiribocchi A 2020 *Scientific Reports* **10** 15936
- [15] Favuzzi I, Carenza L, Corberi F, Gonnella G, Lamura A and Negro G 2021 *Soft Materials* **19** 334–345 URL <https://doi.org/10.1080/1539445X.2021.1908357>
- [16] Giordano M G, Bonelli F, Carenza L N, Gonnella G and Negro G 2021 *Europhysics Letters* **133** 58004 URL <https://dx.doi.org/10.1209/0295-5075/133/58004>
- [17] Head L C, Doré C, Keogh R R, Bonn L, Negro G, Marenduzzo D, Doostmohammadi A, Thijssen K, López-León T and Shendruk T N 2024 *Nature Physics* 1–9
- [18] Vicsek T and Zafeiris A 2012 *Physics reports* **517** 71–140 URL <https://doi.org/10.1016/j.physrep.2012.03.004>
- [19] GrandPre T and Limmer D T 2018 *Physical Review E* **98**(6) 060601 URL <https://doi.org/10.1103/PhysRevE.98.060601>
- [20] Negro, G, Caporusso, C B, Digregorio, P, Gonnella, G, Lamura, A and Suma, A 2022 *Eur. Phys. J. E* **45** 75 URL <https://doi.org/10.1140/epje/s10189-022-00230-1>
- [21] Caporusso C B, Negro G, Suma A, Digregorio P, Carenza L N, Gonnella G and Cugliandolo L F 2024 *Soft Matter* **20**(4) 923–939 URL <http://dx.doi.org/10.1039/D3SM01030A>
- [22] Tailleur J and Cates M E 2008 *Phys. Rev. Lett.* **100**(21) 218103 URL <https://link.aps.org/doi/10.1103/PhysRevLett.100.218103>
- [23] Cates M E and Tailleur J 2015 *Annu. Rev. Condens. Matter Phys.* **6** 219–244 URL <https://doi.org/10.1146/annurev-conmatphys-031214-014710>
- [24] Caporusso C B, Digregorio P, Levis D, Cugliandolo L F and Gonnella G 2020 *Physical Review*

- Letters* **125**(17) 178004 URL <https://doi.org/10.1103/PhysRevLett.125.178004>
- [25] Fily Y, Henkes S and Marchetti M C 2014 *Soft Matter* **10**(13) 2132–2140
- [26] Cugliandolo L F, Digregorio P, Gonnella G and Suma A 2017 *Physical Review Letters* **119**(26) 268002 URL <https://doi.org/10.1103/PhysRevLett.119.268002>
- [27] Digregorio P, Levis D, Suma A, Cugliandolo L F, Gonnella G and Pagonabarraga I 2018 *Physical Review Letters* **121**(9) 098003 URL <https://doi.org/10.1103/PhysRevLett.121.098003>
- [28] Petrelli I, Digregorio P, Cugliandolo L F, Gonnella G and Suma A 2018 *The European Physical Journal E* **41** 1–23 URL <https://doi.org/10.1140/epje/i2018-11739-y>
- [29] Cagnetta F, Corberi F, Gonnella G and Suma A 2017 *Physical review letters* **119** 158002 URL <https://doi.org/10.1103/PhysRevLett.119.158002>
- [30] Gradenigo G and Majumdar S N 2019 *Journal of Statistical Mechanics: Theory and Experiment* **2019** 053206 URL <https://dx.doi.org/10.1088/1742-5468/ab11be>
- [31] Semeraro M, Gonnella G, Suma A and Zamparo M 2023 *Physical Review Letters* **131**(15) 158302 URL <https://doi.org/10.1103/PhysRevLett.131.158302>
- [32] Seifert U 2012 *Reports on Progress in Physics* **75** 126001 URL <https://doi.org/10.1088/0034-4885/75/12/126001>
- [33] Peliti L and Pigolotti S 2021 *Stochastic Thermodynamics: An Introduction* (Princeton University Press) URL <https://press.princeton.edu/books/hardcover/9780691201771/stochastic-thermodynamics>
- [34] Shiraishi N 2023 *An Introduction to Stochastic Thermodynamics: From Basic to Advanced* vol 212 (Springer Nature) URL <https://link.springer.com/book/10.1007/978-981-19-8186-9>
- [35] Fodor E, Jack R L and Cates M E 2021 Irreversibility and biased ensembles in active matter: Insights from stochastic thermodynamics (*Preprint* 2104.06634)
- [36] O’Byrne J, Kafri Y, Tailleur J and van Wijland F 2022 *Nature Reviews Physics* **4**(3) 167183 URL <https://doi.org/10.1038/s42254-021-00406-2>
- [37] Burkholder E W and Brady J F 2019 *The Journal of chemical physics* **150**
- [38] Caprini L, Puglisi A and Sarracino A 2021 *Symmetry* **13** 81
- [39] Cengio S D, Levis D and Pagonabarraga I 2021 *Journal of Statistical Mechanics: Theory and Experiment* **2021** 043201 URL <https://dx.doi.org/10.1088/1742-5468/abee22>
- [40] Loi D, Mossa S and Cugliandolo L F 2008 *Physical Review E* **77**(5) 051111 URL <https://doi.org/10.1103/PhysRevE.77.051111>
- [41] Loi D, Mossa S and Cugliandolo L F 2008 *Phys. Rev. E* **77**(5) 051111 URL <https://link.aps.org/doi/10.1103/PhysRevE.77.051111>
- [42] Nandi S K and Gov N S 2019 *The European Physical Journal E* **41**(10) 117 URL <https://doi.org/10.1140/epje/i2018-11731-7>
- [43] Palacci J, Cottin-Bizonne C, Ybert C and Bocquet L 2010 *Physical Review Letters* **105** 088304 URL <https://doi.org/10.1103/PhysRevLett.105.088304>
- [44] Suma A, Gonnella G, Laghezza G, Lamura A, Mossa A and Cugliandolo L F 2014 *Phys. Rev. E* **90**(5) 052130 URL <https://link.aps.org/doi/10.1103/PhysRevE.90.052130>
- [45] Szamel G 2014 *Phys. Rev. E* **90**(1) 012111 URL <https://link.aps.org/doi/10.1103/PhysRevE.90.012111>
- [46] Levis D and Berthier L 2015 *Europhysics Letters* **111** 60006 URL <https://dx.doi.org/10.1209/0295-5075/111/60006>
- [47] Levis D and Berthier L 2015 *EPL (Europhysics Letters)* **111** 60006 URL <https://doi.org/10.1209/0295-5075/111/60006>
- [48] Petrelli I, Cugliandolo L F, Gonnella G and Suma A 2020 *Phys. Rev. E* **102**(1) 012609 URL <https://link.aps.org/doi/10.1103/PhysRevE.102.012609>
- [49] Gallavotti G and Cohen E G D 1995 *Journal of Statistical Physics* **80** 333–365 URL <https://link.springer.com/article/10.1007/BF02179860#citeas>
- [50] Lebowitz J L and Spohn H 1999 *Journal of Statistical Physics* **95** 333–365 URL <https://link.springer.com/article/10.1023/A:1004589714161>

- [51] Crooks G E 1999 *Phys. Rev. E* **60**(3) 2721–2726 URL <https://link.aps.org/doi/10.1103/PhysRevE.60.2721>
- [52] Harris R J and Schütz G M 2007 *Journal of Statistical Mechanics: Theory and Experiment* **2007** P07020 URL <https://dx.doi.org/10.1088/1742-5468/2007/07/P07020>
- [53] Sevick E, Prabhakar R, Williams S R and Searles D J 2008 *Annual Review of Physical Chemistry* **59** 603–633 pMID: 18393680 URL <https://doi.org/10.1146/annurev.physchem.58.032806.104555>
- [54] Dabelow L, Bo S and Eichhorn R 2019 *Phys. Rev. X* **9**(2) 021009 URL <https://link.aps.org/doi/10.1103/PhysRevX.9.021009>
- [55] Bodineau T and Derrida B 2007 *Comptes Rendus Physique* **8** 540–555 ISSN 1631-0705 work, dissipation, and fluctuations in nonequilibrium physics URL <https://doi.org/10.1016/j.crhy.2007.04.014>
- [56] Dembo A and Zeitouni O 1988 *Large Deviations Techniques and Applications* 2nd ed (Springer - New York) URL <https://link.springer.com/book/10.1007/978-3-642-03311-7>
- [57] den Hollander F 2000 *Large Deviations* (AMS) URL <https://bookstore.ams.org/sza/view?ProductCode=FIM/14>
- [58] Touchette H 2009 *Physics Reports* **478** 1–69 ISSN 0370-1573 URL <https://www.sciencedirect.com/science/article/pii/S0370157309001410>
- [59] Visco P 2006 *Journal of Statistical Mechanics: Theory and Experiment* **2006** P06006–P06006 URL <https://doi.org/10.1088/1742-5468/2006/06/p06006>
- [60] Fogedby H C and Imparato A 2011 *Journal of Statistical Mechanics: Theory and Experiment* **2011** P05015 URL <https://doi.org/10.1088/1742-5468/2011/05/p05015>
- [61] Loi D, Mossa S and Cugliandolo L F 2008 *Phys. Rev. E* **77**(5) 051111
- [62] Ben-Isaac E, Park Y, Popescu G, Brown F L H, Gov N S and Shokef Y 2011 *Phys. Rev. Lett.* **106**(23) 238103
- [63] Dieterich E, Camunas-Soler J, Ribezzi-Crivellari M, Seifert U and Ritort F 2015 *Nature Physics* **11** 971–977
- [64] Nandi S K and Gov N 2018 *The European Physical Journal E* **41** 1–5
- [65] Cugliandolo L F, Gonnella G and Petrelli I 2019 *Fluctuation and Noise Letters* **18** 1940008
- [66] Mandal S, Liebchen B and Löwen H 2019 *Phys. Rev. Lett.* **123**(22) 228001 URL <https://doi.org/10.1103/PhysRevLett.123.228001>
- [67] Bonilla L L 2019 *Physical Review E* **100**(2) 022601 URL <https://doi.org/10.1103/PhysRevE.100.022601>
- [68] Caprini L and Marconi U M B 2021 *Journal of Chemical Physics* **154**
- [69] Martin D, O’Byrne J, Cates M E, Fodor E, Nardini C, Tailleur J and van Wijland F 2021 *Phys. Rev. E* **103**(3) 032607 URL <https://link.aps.org/doi/10.1103/PhysRevE.103.032607>
- [70] Semeraro M, Suma A, Petrelli I, Cagnetta F and Gonnella G 2021 *Journal of Statistical Mechanics: Theory and Experiment* **2021** 123202 URL <https://doi.org/10.1088/1742-5468/ac3d37>
- [71] Sekimoto K 2010 *Stochastic Energetics* (Springer) URL <https://link.springer.com/book/10.1007/978-3-642-05411-2>
- [72] Kanwal R P 2012 *Generalized functions theory and technique: Theory and technique* (Springer Science & Business Media) URL <https://link.springer.com/book/10.1007/978-1-4684-0035-9>
- [73] Abramowitz M and Stegun I A 1972 *Handbook of Mathematical Functions with Formulas, Graphs, and Mathematical Tables. National Bureau of Standards Applied Mathematics Series 55. Tenth Printing.* (ERIC) URL <https://eric.ed.gov/?id=ED250164>
- [74] Caprini L, Marini Bettolo Marconi U, Puglisi A and Vulpiani A 2019 *The Journal of Chemical Physics* **150** 024902 URL <https://doi.org/10.1063/1.5080537>
- [75] Das S, Gompper G and Winkler R G 2018 *New Journal of Physics* **20** 015001 URL <https://dx.doi.org/10.1088/1367-2630/aa9d4b>
- [76] Jiang H R, Yoshinaga N and Sano M 2010 *Physical Review Letters* **105**(26) 268302 URL

- <https://doi.org/10.1103/PhysRevLett.105.268302>
- [77] Theurkauff I, Cottin-Bizonne C, Palacci J, Ybert C and Bocquet L 2012 *Physical Review Letters* **108**(26) 268303 URL <https://doi.org/10.1103/PhysRevLett.108.268303>
- [78] Buttinoni I, Bialké J, Kümmel F, Löwen H, Bechinger C and Speck T 2013 *Physical Review Letters* **110**(23) 238301 URL <https://doi.org/10.1103/PhysRevLett.110.238301>
- [79] Walther A and Müller A H 2008 *Soft matter* **4** 663–668
- [80] Wang G, Sevick E M, Mittag E, Searles D J and Evans D J 2002 *Physical Rev. Lett.* **89** 050601 URL <https://doi.org/10.1103/PhysRevLett.89.050601>
- [81] Blickle V, Speck T, Helden L, Seifert U and Bechinger C 2006 *Physical Review Letters* **96**(7) 070603 URL <https://doi.org/10.1103/PhysRevLett.96.070603>
- [82] Ben-Isaac E, Fodor E, Visco P, van Wijland F and Gov N S 2015 *Physical Review E* **92**(1) 012716 URL <https://doi.org/10.1103/PhysRevE.92.012716>
- [83] Hänggi P, Talkner P and Borkovec M 1990 *Rev. Mod. Phys.* **62**(2) 251–341 URL <https://doi.org/10.1103/RevModPhys.62.251>
- [84] Caprini L, Cecconi F and Marini Bettolo Marconi U 2021 *The Journal of Chemical Physics* **155** 234902 ISSN 0021-9606 (*Preprint* https://pubs.aip.org/aip/jcp/article-pdf/doi/10.1063/5.0074072/13625527/234902_1_online.pdf) URL <https://doi.org/10.1063/5.0074072>
- [85] Stratonovich R L 1967 *Topics in the theory of random noise* vol 2 (CRC Press) URL <https://archive.org/details/stratonovich-topics-in-the-theory-of-random-noise-vol-1>
- [86] Pietzonka P, Fodor E, Lohrmann C, Cates M E and Seifert U 2019 *Physical Review X* **9**(4) 041032 URL <https://doi.org/10.1103/PhysRevX.9.041032>
- [87] Keta Y E, Fodor É, van Wijland F, Cates M E and Jack R L 2021 *Physical Review E* **103** 022603 URL <https://doi.org/10.1103/PhysRevE.103.022603>
- [88] Tuckerman M 2023 *Statistical mechanics: theory and molecular simulation* (Oxford university press) URL <https://global.oup.com/academic/product/statistical-mechanics-theory-and-molecular-simulation-9780198825562>
- [89] Kloeden P E and Platen E 1992 *Numerical Solution of Stochastic Differential Equations* (Springer) URL <https://link.springer.com/book/10.1007/978-3-662-12616-5>
- [90] Risken H 2021 *The Fokker-Planck Equation - Methods of Solution and Applications* 2nd ed (Springer-Verlag)
- [91] Van Kampen N G 1981 *Journal of Statistical Physics* **24** 175–187 URL <https://doi.org/10.1007/BF01007642>
- [92] Arnold P 2000 *Physical Review E* **61**(6) 6091–6098 URL <https://link.aps.org/doi/10.1103/PhysRevE.61.6091>
- [93] Dabelow L, Bo S and Eichhorn R 2021 *Journal of Statistical Mechanics: Theory and Experiment* **2021** 033216 URL <https://doi.org/10.1088/1742-5468/abe6fd>
- [94] Alonso M and Finn E J 1967 *Fundamental university physics* vol 2 (Addison-Wesley Reading, MA) URL <http://www.ii.uib.no/~nicolas/edu/i124/final.rtf>
- [95] Kubo R 1966 *Reports on Progress in Physics* **29** 255–284 URL <https://doi.org/10.1088/0034-4885/29/1/306>